Icarus 297 (2017) 160–178

Contents lists available at ScienceDirect

Icarus

journal homepage: www.elsevier.com/locate/icarus

Inhibition of ordinary and diffusive convection in the water condensation zone of the ice giants and implications for their thermal evolution

A James Friedson[a,*], Erica J. Gonzales[b,c]

[a] Jet Propulsion Laboratory, California Institute of Technology, USA
[b] 2012 Summer Undergraduate Research Fellow, Jet Propulsion Laboratory, California Institute of Technology, USA
[c] Department of Physics, University of Notre Dame, USA

ARTICLE INFO

Article history:
Received 26 July 2016
Revised 22 June 2017
Accepted 26 June 2017
Available online 30 June 2017

ABSTRACT

We explore the conditions under which ordinary and double-diffusive thermal convection may be inhibited by water condensation in the hydrogen atmospheres of the ice giants and examine the consequences. The saturation of vapor in the condensation layer induces a vertical gradient in the mean molecular weight that stabilizes the layer against convective instability when the abundance of vapor exceeds a critical value. In this instance, the layer temperature gradient can become superadiabatic and heat must be transported vertically by another mechanism. On Uranus and Neptune, water is inferred to be sufficiently abundant for inhibition of ordinary convection to take place in their respective condensation zones. We find that suppression of double-diffusive convection is sensitive to the ratio of the sedimentation time scale of the condensates to the buoyancy period in the condensation layer. In the limit of rapid sedimentation, the layer is found to be stable to diffusive convection. In the opposite limit, diffusive convection can occur. However, if the fluid remains saturated, then layered convection is generally suppressed and the motion is restricted in form to weak, homogeneous, oscillatory turbulence. This form of diffusive convection is a relatively inefficient mechanism for transporting heat, characterized by low Nusselt numbers. When both ordinary and layered convection are suppressed, the condensation zone acts effectively as a thermal insulator, with the heat flux transported across it only slightly greater than the small value that can be supported by radiative diffusion. This may allow a large superadiabatic temperature gradient to develop in the layer over time. Once the layer has formed, however, it is vulnerable to persistent erosion by entrainment of fluid into the overlying convective envelope of the cooling planet, potentially leading to its collapse. We discuss the implications of our results for thermal evolution models of the ice giants, for understanding Uranus' anomalously low intrinsic luminosity, and for inducing episodes of intense convection in the atmospheres of Saturn, Uranus, and Neptune.

1. Introduction

The accretion of the outer planets is generally believed to have formed them with high initial temperatures and they have been slowly releasing the primordial heat of their formation over the age of the solar system. Historically, thermal evolution models of Uranus and Neptune have encountered difficulty in reproducing their present effective temperatures. Their current (4.6 Gy) effective temperatures could be explained only if they started with relatively low internal entropies, suggesting a "cold accretion" scenario for their formation, or if stable compositional stratification in their interiors suppressed convective cooling during some portion of their evolution (Hubbard and McFarlane 1980; Podolak et al., 1991; Hubbard et al., 1995). More recently, taking advantage of new data for the equation of state of water, Fortney et al. (2011) found that they could match the observations of Neptune's effective temperature with a model that included a fully convective interior. However, their model Uranus still cooled too slowly. As others had done previously, they surmised that a strong barrier to convective cooling of the interior has existed on Uranus but not on Neptune.

In these cooling calculations, it has been assumed that the thermal structure inside the planet can be adequately represented by a single adiabat running from the core to just below the visible atmosphere. Although water is predicted to be abundant in the envelopes of the ice giants, the effects of water condensation have not been included in the models.

* Corresponding author.
E-mail address: Andrew.Friedson@jpl.nasa.gov (A.J. Friedson).

http://dx.doi.org/10.1016/j.icarus.2017.06.029
0019-1035/

Table 1
Critical Abundance for Inhibition of Convection. The abundance is given in terms of the factor of enrichment over the solar value that is required. Adapted from Guillot (1995), with solar abundances from Asplund et al. (2009).

Species	Jupiter	Saturn	Uranus	Neptune
CH_4*	–	–	20.9	22.1
NH_3	52.8	54.3	86.8	92.5
H_2O	8.0	8.5	11.0	11.7

* Methane does not condense in Jupiter and Saturn

The purpose of this paper is to examine how water condensation in the deep atmospheres of the ice giants may have affected the cooling of their interiors over the course of their thermal evolution. As will be explained below, the formation of a saturated water layer has the potential to suppress both ordinary and double-diffusive convection within the layer, providing a barrier to convective cooling of the interior. As a result, the layer acts effectively as an imperfect insulator separating the water-rich deep atmosphere below from a relatively cold, dry atmosphere above. The insulating effect of this gradient zone allows the atmosphere above and below to lie on potentially very different adiabats connected by a superadiabatic temperature gradient. In this way, incorporation of the effect of water condensation in ice giant cooling models may fundamentally alter calculated cooling trajectories by altering the relationship existing between the effective temperature of the planet at any given time and the entropy stored in its deep atmosphere and interior.

The most abundant species able to condense in the atmospheres of the outer planets all have molecular weights much larger than that of hydrogen and helium, the two principal components of the dry air. Guillot (1995) demonstrated that condensation of these species could inhibit moist convection within a saturated layer provided their abundance at the base of the layer exceeds a critical value. If it does, then a region near the base of the layer becomes stable to convection as a consequence of the density stratification imparted by the mean molecular weight gradient induced by the decreasing mixing ratio of the saturated species. Under such conditions, a layer possessing a superadiabatic temperature gradient becomes buoyantly stable. With ordinary convection inhibited, heat must be transported through the gradient zone by a less efficient mechanism, such as by double-diffusive convection or radiation.

Table 1 lists the critical abundances for CH_4, NH_3, and water in the atmospheres of the outer planets. The data are taken from Guillot (1995). The abundances are given in terms of the enrichment of the C, N, or O mole fraction relative to solar composition (Asplund et al., 2009). The modest enrichments of NH_3 observed in Jupiter and Saturn (Atreya et al., 2003; Briggs and Sackett 1989) are much lower than the critical values shown in the table. Therefore ammonia condensation should not be effective in inhibiting convection in these planets. In contrast, the best estimates for the methane abundances observed on Uranus and Neptune exceed ~35 times solar (Sromovsky et al., 2011; Baines et al., 1995), well above their critical values. Guillot (1995) concluded that moist convection is inhibited where the methane saturates. A similar conclusion can be drawn for the water condensation layer in these planets if their oxygen abundance is supercritical, and the degree that carbon is enriched over solar suggests that this may well be likely. Interior models of Uranus and Neptune, constrained by the gravity field measurements, generally favor solutions having water abundances in the molecular envelope that are several times the critical value (Fortney and Nettelmann 2010). This opens the possibility that condensation of water may have played an important role in inhibiting internal cooling in the ice giants during the course of their thermal evolution.

The abundances of water in the deep atmospheres of Jupiter and Saturn are unknown. If oxygen is at least as enriched over the solar value as carbon in these planets (i.e, between ~4 to 10 times solar), then it is possible that water condensation can potentially inhibit convection in these atmospheres as well. However, the criterion for convective inhibition is likely to be only marginally satisfied. As will be shown below, this implies that stable layers formed in this way would be relatively quite thin and therefore especially susceptible to erosion and catastrophic failure. Consequently, we do not expect formation of saturated water zones in Jupiter and Saturn substantially affected their cooling histories. Effects associated with the molecular weight of water may nevertheless have observable consequences for the dynamics of moist convection in Saturn (Li and Ingersoll 2015).

In Section 2, we discuss the inhibition of ordinary moist convection in the water condensation zone, introduce the dynamical equations we use to calculate motion associated with buoyancy in the layer, and explore the stability of the layer to infinitesimal upward and downward displacements in the absence of viscosity and thermal diffusion. In Section 3, we set up the linear perturbation equations that govern small-amplitude motions and investigate the conditions for which viscosity and thermal (radiative) diffusion lead to instability to double-diffusive convection. We find that diffusive convection in the condensation layer is suppressed in the limit where the condensate precipitates rapidly out of the system.

In a contemporaneous study, Leconte et al. (2017) also explore the inhibition of double-diffusive convection in the condensation layers of hydrogen-rich atmospheres. They find, as we do, that diffusive convection can be suppressed in the condensation zone if the condensable species is sufficiently abundant, provided the condensate is rapidly removed from buoyant fluid elements where condensation occurs.

Leconte et al. (2017) do not perform an analogous calculation examining the opposite extreme, where rainout of the condensate is assumed to proceed very slowly. We find that the layer can undergo diffusive convection when the motion of condensed droplets is tightly coupled to that of the gas (that is, in the limit of slow precipitation). In Section 4, we explore whether the ensuing diffusive instability takes the form of disorganized, homogeneous turbulence or organizes into layered convection. A discussion of the potential implications of our results for the cooling histories of Uranus and Neptune is offered in Section 5; in particular, we consider the ability of a stable layer, once formed, to resist persistent, erosive entrainment of its fluid into the overlying convective envelope as the outermost layers of the planet continue to cool. We summarize our conclusions in Section 6.

2. Inhibition of moist convection in the water condensation zone

In Earth's atmosphere, the vertical density stratification is dominated by the vertical temperature variation; variation in the water mixing ratio has only a weak effect. This is because the water mixing ratio is relatively low and because water is lighter than nitrogen. In the outer planets, saturation of vapor in a condensation zone sets up a vertical gradient in the mean molecular weight of the air (Guillot 1995). If the vapor is sufficiently abundant, the gradient can stabilize the layer against moist convection. This can be seen by considering the buoyancy force acting on a parcel of fluid displaced vertically in a saturated layer in which the temperature decreases with altitude faster than the moist pseudoadiabat. As the parcel rises, its temperature follows the pseudoadiabat, it becomes warmer than its surroundings, and if there were no molecular weight effect, it would become positively buoyant. However, by virtue of being warmer than its surroundings, it also

holds more saturated vapor, which contributes negative buoyancy. If the saturation mixing ratio is sufficiently high, the net buoyancy force opposes the vertical displacement and convection becomes inhibited.

The basic equations that govern motion driven by buoyancy in the condensation zone consist of the momentum (1a–1c) and continuity (1d) equations, the second law of thermodynamics (1e), the equation of state (1f), and the budget for the specific humidity (1g), expressed in Cartesian coordinates in which x and y lie in the horizontal plane and z is altitude:

$$\frac{du}{dt} + \frac{1}{\rho}\frac{\partial p}{\partial x} = \nu\nabla^2 u \tag{1a}$$

$$\frac{d\upsilon}{dt} + \frac{1}{\rho}\frac{\partial p}{\partial y} = \nu\nabla^2 \upsilon \tag{1b}$$

$$\frac{dw}{dt} + \frac{1}{\rho}\frac{\partial p}{\partial z} + g = \nu\nabla^2 w \tag{1c}$$

$$\frac{1}{\rho}\frac{d\rho}{dt} = -\left(\frac{\partial u}{\partial x} + \frac{\partial w}{\partial z}\right) \tag{1d}$$

$$\frac{1}{T}\frac{dT}{dt} - \frac{R}{C_p}\frac{1}{p}\frac{dp}{dt} = -\frac{L}{C_p T}\frac{1}{1-q-l}(E-C) + \frac{\kappa_r}{T}\nabla^2 T \tag{1e}$$

$$\frac{1}{\rho}\frac{d\rho}{dt} = -\frac{1}{T}\frac{dT}{dt} + \frac{1}{p}\frac{dp}{dt} - \frac{1-f_c+\xi}{1+\xi q - l(1-f_c)}\frac{dq}{dt}. \tag{1f}$$

$$\frac{dq}{dt} = E - C + D_q\nabla^2 q \tag{1g}$$

In these equations, t is time; u, υ, and w represent the horizontal and vertical velocity components; p is pressure; T, temperature; ρ, mass density; q, specific humidity; and l, the mass mixing ratio of condensate. The advective derivative, $d/dt \equiv \partial/\partial t + \mathbf{v}\cdot\nabla$, expresses the rate of change following an element of fluid. In Eqs. (1e) and (1g), E and C represent the sources and sinks of specific humidity associated with evaporation and condensation, respectively. Other notation includes the surface gravity g; gas constant R and specific heat, C_p for the hydrogen-helium-water mixture; water's latent heat of vaporization L; and the viscosity ν and effective thermal diffusivity κ_r of the system. D_q is the local diffusivity of water through hydrogen. During the interval of thermal evolution in the ice giants of primary interest here, the base of the water cloud occurs at tens to hundreds of bars. At these pressures we expect the diffusive transport of heat to be dominated by a random walk of photons through windows in the spectrum where the opacity is lowest; thus κ_r here represents the thermal diffusivity associated with the radiative conductivity determined by the local Rosseland mean opacity (Guillot et al., 1994).

The coupling of the specific humidity to the mean molecular weight of the air occurs through the parameter $\xi = 1/\varepsilon_v - 1$ in Eq. (1f), where ε_v is the ratio of the molecular weight of the vapor to that of the dry air. For water vapor in the ice giants, $\varepsilon_v \cong 7.8$ and $\xi = -0.87$. For negative values of ξ, adding water causes the mean molecular weight of a fluid parcel to increase.

In Eq. (1f), we have introduced a parameter, f_c, as a device to switch between two limiting cases. It has a value of either 0 or 1 only. The cases are defined by the relative magnitudes of the characteristic vertical velocity of the buoyancy oscillations and the sedimentation velocity of condensed particles. In the limit where the characteristic buoyancy velocity is small in comparison to the sedimentation velocity, the particles separate from the fluid quickly and do not substantially affect the overall buoyancy of the fluid parcel in which they condensed. The parcel's density is then controlled entirely by changes in its saturated specific humidity. This approximation is the one invoked to derive the moist pseudoadiabatic lapse rate and also corresponds to the assumption adopted by Guillot (1995). It is captured in Eq. (1f) by setting $f_c = 1$. In the opposite extreme, the condensate remains suspended and approximately moves with the fluid parcel in which it condensed over an interval of many buoyancy periods. This case is captured in Eq. (1f) by setting $f_c = 0$. In deriving (1f) for this limit, we have made the tacit assumption that the parcel remains saturated and that it does not exchange mass with the environment; hence $dl = -dq$ in the parcel at all times. This assumption can be valid only if there is enough *total* water in the parcel initially to ensure that l always remains positive during the motion. For small-amplitude motion, this does not require a significant initial abundance of condensate, and therefore adopting the above assumption is not necessarily too restrictive. In this paper, we analyze the stability of the condensation zone for both the rapid and slow precipitation limits.

A basic criterion can be derived for the local stability of a saturated layer possessing a strong vertical gradient of mean molecular weight by considering the buoyancy force that develops when an element of fluid is given a small vertical displacement from its original position. If the buoyancy force acts in the direction of the displacement, the perturbation is reinforced and the layer is unstable; otherwise it is stable. In a saturated layer, the air of ascending elements remains saturated, condensation occurs, and latent heat is released. When the condensate can be considered to precipitate rapidly out of the system, the air in descending elements is unsaturated and the specific humidity is conserved following the motion. Consequently, the criterion for stability of the saturated layer to a small displacement in this limit depends on whether the displacement is upward or downward and separate criteria must be derived for the two cases. A layer in Earth's atmosphere is referred to as "conditionally unstable" if it is unstable to upward displacements but stable to downward displacements. On the other hand, when the condensate remains suspended in the fluid element for several buoyancy periods, the criterion for stability does not depend on whether the displacement is upward or downward.

In Appendix A, we derive the criteria for the stability of a saturated layer to small upward and downward displacements, for both the fast and slow precipitation limits. At this stage, the effects of momentum, heat, and water diffusion are ignored; their influence on the stability is considered in the next section. For an *upward* displacement in the fast precipitation limit, one finds the layer is stable when

$$\alpha\left(\frac{\partial T_0}{\partial z} + \Gamma_s\right) > 0 \tag{2}$$

where T_0 is the environmental temperature, and Γ_s is the moist pseudoadiabatic lapse rate (see Equation [A7] for the relationship between Γ_s and the dry adiabat $\Gamma_d = g/C_p$). The parameter α is given by

$$\alpha = 1 + \xi\,(q_s L/R_w T_0) \tag{3}$$

where R_w is the gas constant for pure water and q_s is the saturation specific humidity. When $\alpha \approx 1$, the molecular weight gradient does not play an important role and the formula reduces to the usual criterion for stability of an atmosphere against moist convection. In the gaseous outer planets, α can become negative in the saturation layer if q_s becomes sufficiently large. When α is negative, the usual stability criterion is turned on its head; superadiabatic lapse rates become stable and subadiabatic lapse rates become unstable. However, convection generated in a subadiabatic environment under these circumstances must be short-lived, since it transports heat and vapor *downward* and drives the lapse rate toward the moist adiabat. Consequently, convection in a subadiabatic saturated layer cannot participate in transporting heat outward in the planet. The endurance of a stable, superadiabatic gradient zone,

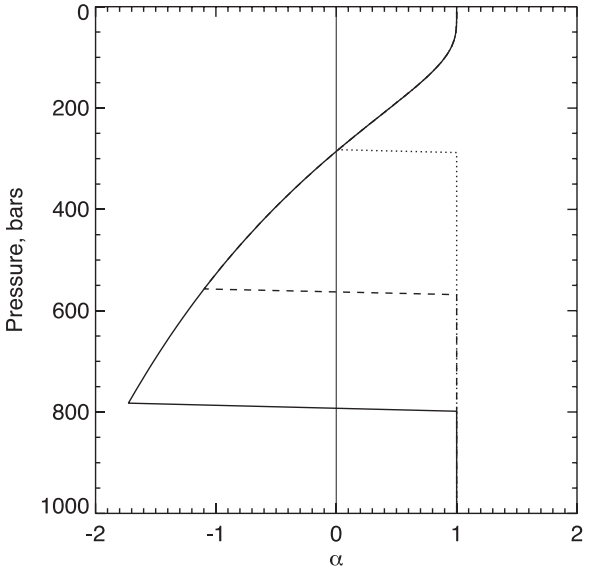

Fig. 1. Vertical profiles of α for Uranus for three values of the mole fraction of water in the deep atmosphere below the saturation layer: 1.4% (dotted); 4.3% (dashed); and 7.2% (solid). Convection is inhibited at the pressures for which α is less than zero for each case. In this model, convection is not inhibited at any depth if the deep water abundance is less than ~1.4%. Note that the base of the saturated layer cannot extend deeper than the level where the temperature exceeds the critical temperature of water (~647 K). .

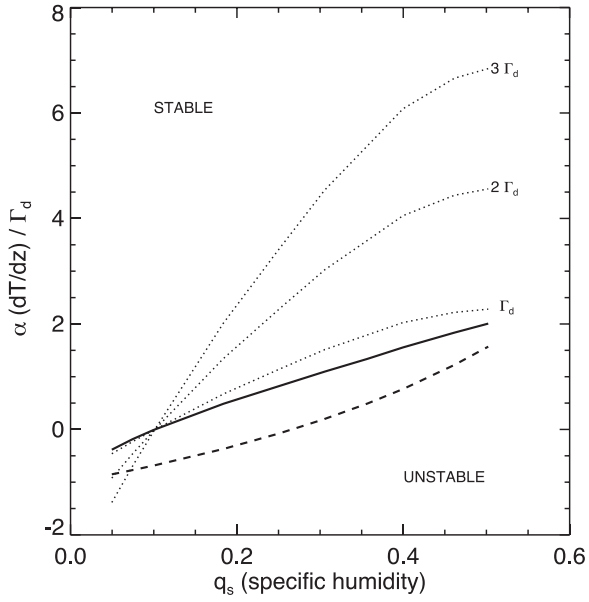

Fig. 2. Stability of the water condensation zone based on the present-day Uranus thermal profile used to construct Fig 1. The product of α with the temperature gradient (normalized by the dry adiabatic lapse rate) is plotted as a function of the specific humidity in the deep atmosphere at the base of the water cloud. Condensates are assumed to precipitate rapidly out of a rising plume. The solid line corresponds to the neutral stability condition for a saturated upward displacement and the dashed line to the neutral stability condition for a dry downward displacement. Lapse rates that fall above the solid line for a given specific humidity are stable to both upward and downward displacements whereas those that fall below the dashed line are unstable. The dotted curves indicate where constant lapse rates of 1, 2, and 3 times the dry adiabatic lapse rate (Γ_d) fall within the diagram.

on the other hand, will depend on how thick it is and how quickly it is eroded by processes such as convective penetration or drying through precipitation.

The criterion for the stability of a saturated layer to a *downward* displacement in the fast precipitation limit is given by (see Appendix A)

$$\alpha \frac{\partial T_0}{\partial z} + \left(1 - \frac{C_p}{R}\beta\zeta\right)\Gamma_d > 0 \tag{4}$$

Here, we have defined $\zeta \equiv \xi/(1+\xi q_0)$ and $\beta \equiv p_0(\partial q_s/\partial p)_{T,0}$ accounts for the dependence of the saturation specific humidity on the local pressure. Where α is negative, large lapse rates promote the stability of the layer to a downward displacement of fluid, and superadiabatic gradients therefore once again are associated with stable stratification. Eq. (4) corresponds to the Ledoux criterion (Ledoux 1947) for the stability of a layer possessing a mean molecular weight gradient equal to that provided by the saturation profile of water in a hydrogen-dominated atmosphere.

Fig. 1 shows the vertical variation of α associated with water condensation in a model of Uranus' current atmosphere. The temperature profile at pressures greater than 10 bars is taken to follow a moist pseudoadiabat (which collapses onto a dry adiabat at pressures where the air is unsaturated or where moist effects are negligible). At the temperatures and pressures of interest, conversion between the ortho and para forms of hydrogen is relatively rapid and therefore ortho-para hydrogen conversion does not significantly affect the nature of the convection (Conrath and Gierasch 1984). The temperature profile has been calculated by assigning a temperature of 147 K to the 10 bar level (extrapolated adiabatically from the Voyager radio occultation profile, Lindal et al., 1987) and integrating downward to solve for the temperatures lying on the moist adiabat at higher pressures while simultaneously solving for the moist pseudoadiabatic lapse rate and saturated specific humidity implied by the local temperature. Below the base of the water cloud, the temperature profile follows a dry adiabat and the specific humidity is assumed to be constant with depth. This thermal profile corresponds to the "classical" model for the structure of Uranus' deep atmosphere, in the sense that the possible presence of a stable superadiabatic gradient zone has not been included in the calculation. Vertical profiles of α are shown for three assumed values for the deep water mole fraction: 1.4%, 4.3%, and 7.2%, which correspond respectively to 17, 51, and 87 times that based on the solar photospheric abundance of oxygen (Asplund et al., 2009). Eqs. (2) and (4) indicate that ordinary moist convection is inhibited and a superadiabatic lapse rate is locally stable at levels where α is negative. Under such conditions, the heat must be transported radially by a less efficient mechanism, such as by radiation or diffusive convection. When the mole fraction of water in the deep atmosphere is 1.4% or less, α in the model is never negative and water saturation does not inhibit convection. For the cases with mole fractions of 4.3% and 7.2%, we see the development of thick layers where α is negative starting above 560 bars and 780 bars, respectively. In reality, the profiles shown in Fig. 1 overestimate the vertical extent of these layers, because the effect of the superadiabatic lapse rate that would develop in these layers, which has not been included in this calculation, is to thin the layers by imparting a smaller scale height to the saturation mixing ratio. Nevertheless, it is clear from these profiles that inhibition of convection in the condensation zone is very likely to occur in the ice giants, both in their current state and at earlier stages in their history, if their water abundance below the saturation zone exceeds about 20 times solar. Current interior models favor significantly higher values for the water abundance on both planets (Fortney and Nettelmann 2010).

Fig. 2 shows an example of how the stability of a saturated layer varies with the specific humidity and lapse rate. For this example, we use the thermal profile for present-day Uranus to relate the temperature to the pressure and specific humidity at the base of the water cloud. The solid curve corresponds to the stability boundary for saturated upward parcel displacements and the dashed curve to dry downward displacements. Points lying above

the solid curve correspond to combinations of specific humidity and lapse rate that are stable and points below the dashed curve to combinations that are unstable. Points lying between the dashed and solid curves correspond to conditionally unstable stratification. For specific humidities greater than ~0.1, α is negative and lapse rates greater than the moist pseudoadiabat (indicated by the solid line in the diagram) are stable. In addition, for a given specific humidity at the base of the gradient zone, increasing the lapse rate increases the stability. This runs counter to our experience with the terrestrial atmosphere, where the opposite is true, and arises entirely through the introduction of a strong vertical gradient of mean molecular weight by the saturated vapor profile.

We may also derive the stability criterion for the case where condensate precipitation is slow and particles follow the fluid motion closely for several buoyancy periods. The derivation is presented in Appendix A (see Eq. (A13)). The criterion is found to be very similar to that given in (4) and closely tracks the dashed line when plotted in Fig. 2. However, whereas the criterion in (4) applies only for downward parcel displacements, the criterion given in (A13) applies for both upward and downward displacements. Consequently, we see that slow precipitation of condensate effectively increases the static stability of the system, all other parameters being equal.

It is of interest as well to consider the nature of the heat transfer for a configuration consisting of dry air sitting on top of a moist interior, the two regions separated by a thin interface at the base of the condensation zone. Such a configuration corresponds to the limiting case of a condensation zone that has been efficiently dried by sustained turbulence arising from, for example, diffusive convection. (We discuss such a scenario in Section 5). The large negative gradient of mean molecular weight across the interface ensures that it is locally stable to overturning. However, heat may still be transferred convectively if the convective plumes are energetic enough to overshoot the region of negative buoyancy to an altitude where they become positively buoyant. A water-rich parcel displaced pseudoadiabatically upward across the interface will initially be negatively buoyant because it holds more water than the relatively dry environment and because, when α is negative, the stabilizing effect of the molecular weight gradient outweighs the destabilizing effect of latent heat release. Upon further upward displacement, however, the parcel will eventually become buoyant as it dries through precipitation and is warmed by latent heating. Applying the same methods used to derive the stability criteria given above, it is possible to estimate the work per unit mass that must be done against buoyancy to lift the parcel to the height of neutral stability, and to compare it to the order of magnitude of the kinetic energy per unit mass available in the convection below the condensation level. The latter can be estimated as $\sim (F/\rho_0)^{2/3}$, where F is the convective heat flux in the ice giant interior below the condensation zone and ρ_0 is the local mass density. If the work that must be done is much larger than the available kinetic energy, then penetration of convective plumes to their level of neutral buoyancy will be energetically unfavorable (Guillot 1995). Our estimates show that this will in fact be the case. For example, for a deep water mole fraction of 4.3% ($q_s = 0.25$), the work required is more than five orders of magnitude greater than the kinetic energy of the convection, even for the case when the ice giants were young and had intrinsic heat flows as high as $\sim 10\,\mathrm{W\,m^{-2}}$, or 25 times Neptune's present internal heat flux (Pearl and Conrath 1991).

We conclude that the water condensation zone in the ice giants acts effectively as a barrier to radial heat transfer by moist convection, irrespective of whether the zone is fully saturated, provided the abundance of water in the atmosphere below the condensation zone is sufficiently high. This does not rule out the possibility, however, that a diffusive interface could form, separating the moist interior from a dry envelope. We discuss this question further in Section 5.

3. Stability of the condensation zone to diffusive convection

If ordinary moist convection is inhibited in the water condensation zone, heat must be transported radially through the layer by another mechanism, such as diffusive convection or radiation. Before we can assess the influence of water condensation on the internal structure and thermal evolution of the ice giants, we must first evaluate the potential efficiency of diffusive-convection as a mechanism for transferring heat through the condensation zone. This is important since, if relatively large diffusive-convective heat fluxes develop for small superadiabatic gradients, the overall effect of water condensation on the thermal evolution of the ice giants would be minor.

Diffusive convection arises as an instability in a system that is thermally unstably stratified but overall stabilized by a strong compositional gradient (Turner 1973; Huppert and Turner 1981). In dry diffusive convection, thermal diffusion causes a parcel displaced upward to be colder and heavier than it would be in the absence of diffusion, and therefore as it descends on the downward leg of its oscillation, it sinks further than it would otherwise. It then diffusively warms, becomes lighter, and rises higher on the upward leg than it would otherwise. This leads to an overdamped oscillation where the amplitude grows slowly with time. Eventually, nonlinear interactions between modes limits further amplitude growth and quasi-steady diffusive convection sets in.

Physical reasoning suggests that a saturated system, characterized by negative α and undergoing a pseudoadiabatic oscillation, will behave somewhat differently. Assuming rapid rainout of droplets, diffusive cooling during uplift causes the parcel to hold less water vapor than it would in the absence of thermal diffusion. When α is negative, the effect of the reduced molecular weight on the parcel's density outweighs the thermal effect, leading to an underdamped oscillation. Under these circumstances we expect the layer will be stable to diffusive convection.

Whether the system actually becomes underdamped depends on whether the condensed droplets become dynamically uncoupled from the gas. During the middle and late stages of their thermal evolution, the base of the water cloud in Uranus and Neptune would have been situated at very high pressures. At these pressures, condensed droplets did not necessarily precipitate rapidly from the updrafts. When droplet precipitation is slow, condensation has little effect on the parcel density and thermal diffusion causes overdamping, as in the dry case. We must therefore consider the possibility that the condensation layer was unstable to diffusive convection when the water cloud was located deep in the atmosphere.

To place the remarks above on a quantitative footing, we consider the linear stability of a superadiabatic, saturated layer with negative α to small-amplitude, plane-wave perturbations. We assume that the basic state atmosphere has zero local wind shear and that the effects of rotation on the perturbations can be neglected. The latter assumption is justified when the ratio of the vertical scale to horizontal scale of the motions is no less than a factor of ~0.1 (Gill 1982). This condition on the aspect ratio will be satisfied if the motions in the stable layer are primarily excited by convective motions in the underlying deep atmosphere that possess horizontal scales comparable to or less than about one scale height. If this is the case then the aspect ratio of motions in the stable layer will be of order unity or greater unless the layer is very shallow. On the other hand, rotation may significantly influence motions with small aspect ratios (large horizontal scales). We do not attempt to model the effects of rotation on such motions in

this study, and the question of the role of rotation in the diffusive-convective stability problem is left open for the present.

We explore the stability of the layer to diffusive convection by linearizing equations (1a) through (1g) about the basic state and searching for the fastest-growing modes. A general perturbation to the dynamical fields can be Fourier-decomposed in terms of normal modes in the form $\psi = \rho_0^{-1/2}\psi_1 \exp\mathrm{i}(kx + mz - \omega t)$, where the real part of ψ represents any of the perturbation variables u', w', or T', and ψ_1 is the corresponding complex amplitude of the perturbation. Similarly, the perturbation pressure is given by $p' = \rho_0^{1/2} p_1 \exp\mathrm{i}(kx + mz - \omega t)$. (Without loss of generality, we may align the horizontal wavenumber with the x-axis and treat the problem as effectively two-dimensional). The horizontal and vertical wavenumber are denoted by k and m, respectively; ω is the (complex) angular frequency of the perturbations. When the imaginary part of ω is positive, the perturbations initially grow exponentially with time and the layer is unstable; otherwise it is stable.

The requirement that the normal modes provide a non-trivial solution to the perturbation equations yields a dispersion relation for ω from which the dependence of the growth rate on wavenumber and other controlling parameters can be determined. For the sake of brevity, we present the derivation of this dispersion relation in Appendix B and here show only the results as they apply to the growth rate. Both the rapid ($f_c = 1$) and slow ($f_c = 0$) precipitation limits are considered.

The dispersion relation takes the form of a cubic equation in ω. The roots of the equation depend on a nondimensional parameter η, the Prandtl number, $\mathrm{Pr} = \nu/\kappa_r$, and the value of f_c. The parameter η is a measure of the ratio of the buoyancy period to the diffusion timescale associated with the wavelength of the perturbation,

$$\eta = \frac{DK^2}{N_a \cos\chi}$$

where $K = (k^2 + m^2 + 1/4H^2)^{1/2}$ with H the local density scale height; N_a is the buoyancy frequency of the stable superadiabatic layer. The orientation of the wavevector of the disturbance is described by the angle χ, defined by

$$\cos\chi = \frac{k}{K}$$

When the effect of finite density scale height can be neglected, χ represents the angle between the wavevector of the perturbation and the x-axis. The generalized diffusion constant D in the expression for η is given by

$$D = \frac{1}{1+\gamma'}\kappa_r + \frac{\gamma'}{1+\gamma'}D_q$$

It thus accounts for the effects of both thermal and molecular diffusion. The parameter $\gamma' = \gamma/(1 - q_0)$, where γ expresses the variation of the saturation specific humidity with temperature and is defined in Appendix A. If we assume a below-cloud water mole fraction of 4.3% in present-day Uranus, the temperature near the cloud base would be approximately 475 K and pressure approximately 430 bars. At this temperature and pressure, the Rosseland-mean opacity can be estimated from the work of Guillot et al. (1994) to be $\sim 5\,\mathrm{cm^2\,g^{-1}}$, implying a radiative diffusivity $\kappa_r \sim 0.07\,\mathrm{cm^2\,s^{-1}}$; the binary diffusion coefficient of water vapor through H_2 is $D_q \sim 3 \times 10^{-3}$ $\mathrm{cm^2\,s^{-1}}$ (Marrero and Mason 1972), the viscosity is $\nu \sim 4 \times 10^{-3}$ $\mathrm{cm^2\,s^{-1}}$ (Forsythe et al. 1954) and we find γ' to be slightly greater than 1. Hence, for these conditions, the Prandtl number is ~0.06 and the dominant contribution to D comes from radiative diffusion. Lower temperatures imply smaller κ_r, higher Prandtl number, and an increasing role for molecular diffusion, whereas lower pressures favor larger κ_r, smaller Prandtl number, and a decreased role for molecular diffusion. We see that small η corresponds to the limit where the influence of diffusion on the motion is weak, whereas large η corresponds to the limit where its influence is strong.

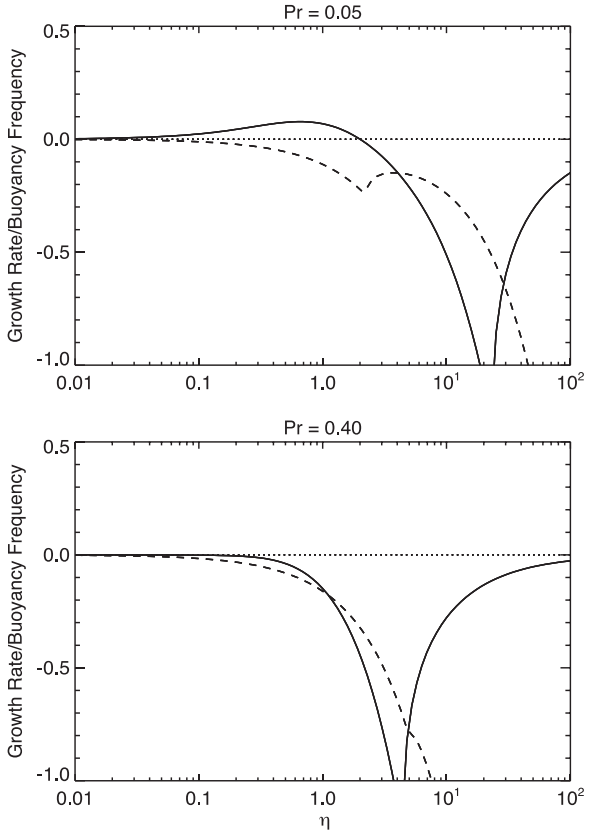

Fig. 3. The maximum growth rate for diffusive-convective instability as a function of η, the ratio of the buoyancy period to the thermal diffusion timescale associated with the wavelength of the perturbation. Positive growth rates indicate instability to a perturbation with the given η. The upper panel is for a layer with Pr = 0.05 and the lower panel for Pr = 0.4. The dashed line corresponds to the fast-precipitation limit ($f_c = 1$) and the solid line to the slow-precipitation limit ($f_c = 0$). The growth rates for the case $f_c = 1$ are shown scaled by a factor of 0.2.

Fig. 3 shows how the maximum growth rate among the three roots of the equation varies with η, for Prandtl numbers of 0.05 and 0.4 and for the slow (f_c equal to 0) and fast (f_c equal to 1) precipitation limits. In all these calculations, we assume $\tau = \mathrm{Pr}$ and γ is chosen such that $\alpha = -1$. We find that in the fast-precipitation limit, the growth rates of the perturbations are negative, irrespective of the value of η or Pr, indicating that condensation causes the normal mode oscillations to be underdamped and the system to be stable against diffusive convection. This result supports the physical argument we made above. However, it comes with a caveat: The calculation for the fast-precipitation limit was carried out under the assumption that the air moving in the downward leg of an oscillation is maintained in a saturated state by evaporation of the condensate yet remains dynamically decoupled from the motion of the particles. This assumption, which has been made solely to render the fast-precipitation case analytically tractable, is lent some support from observations of the downdrafts in terrestrial cloud systems and has been invoked in cumulus parameterization schemes (e.g., Zhang and McFarlane 1995). Its validity for a deep water cloud in an ice giant is far from clear, however, and we must recognize that there may be a "conditional" diffusive-convective instability regime, analogous to the conditional instability regime for ordinary moist convection in Earth's atmosphere, that remains to be explored.

Leconte et al. (2017) have also explored the effect of condensation on the diffusive convective stability of a hydrogen-rich atmosphere. Their calculations differ from ours in several respects. The most important differences are (i) they restrict their attention to the rapid precipitation limit, and (ii) they solve the equations in the Boussinesq approximation, which is applicable when the characteristic vertical length scale of the motion is small in comparison to both the pressure and temperature scale heights. In addition, they neglect the effect of pressure on the saturation equilibrium humidity and focus their attention on the stability of the "elevator mode", for which the motion is entirely in the vertical direction, since it is expected to be the most unstable mode. Finally, in their analysis Leconte et al. (2017) allow for a finite lag time $\tilde{\tau}_c$ for restoring saturation equilibrium after a perturbation, whereas we assume throughout that readjustment to a new equilibrium is effectively instantaneous. Consequently, all the results presented here should be compared only to the $\tilde{\tau}_c = 0$ ("efficient condensation limit") results of Leconte et al. (2017).

Despite the differences between the two calculations, the growth rates of the fastest growing mode found by Leconte et al. (2017) for $\mathrm{Pr} = \tau = 0.01$ (for their case $\tilde{\tau}_c = 0$) are very similar to our results for the fast-precipitation limit for $\mathrm{Pr} = \tau = 0.05$ (dashed curve in Fig. 3). Most importantly, both calculations predict that diffusive convection can be suppressed by condensation in the limit of rapid condensate precipitation.

On the other hand, we find positive growth rates can occur in the slow-precipitation limit, as shown by the solid curve for the case $\mathrm{Pr} = 0.05$ in Fig. 3. Positive growth rates indicate linear instability to diffusive convection. For Prandtl numbers less than ~0.4, a critical value of η exists below which maximum growth rates are positive and above which they are negative. This critical value decreases as Pr increases. For Prandtl numbers greater than ~ 0.4, the maximum growth rate is negative for all η, reflecting the increasing role of viscous damping. Maximum growth rates occur for η of order unity. Perturbations with wavenumbers characterized by this η are overdamped and grow fastest until non-linear interaction between modes or shear instability limits further growth. These results suggest that diffusive convection may become established in the layer when its Prandtl number is relatively low and when particle sedimentation times are long in comparison to the buoyancy period.

As mentioned above, we expect that there would have been an epoch during the cooling of the ice giants when the water condensation zone would have been situated at high pressures, where condensed particle precipitation would have been slow and the Prandtl number would typically have been less than ~0.1. These are the conditions that would have been the most favorable for the onset of diffusive convection. Estimating the likely efficiency of the diffusive convection under these circumstances is the topic of the next section.

4. Character of diffusive convection in the slow-precipitation limit

In the previous section, we have shown that the stability of the water saturation layer to diffusive convection is sensitive to whether the condensate precipitates rapidly or remains suspended, moving with the gas for several buoyancy periods. We find the layer to be stable if the precipitation is relatively rapid and if downdrafts associated with perturbations to the layer are maintained in a saturated state through evaporation. Less clear is the overall stability of the layer when downdrafts are unsaturated; however, we note that diffusive cooling during uplift always promotes underdamping of normal-mode oscillations. In the slow-precipitation limit, the layer is overstable to perturbations whose η are less than a critical value that depends on the Prandtl number of the layer. In this section we examine the likely form diffusive convection takes in the slow-precipitation limit and estimate its potential effectiveness for transferring heat through the layer.

After growth of the initial instability has saturated, the resulting diffusive convection takes the form of either weak homogeneous turbulence or organized layered convection (Rosenblum et al., 2011; Mirouh et al., 2012; Wood et al., 2013). In dry diffusive convection, a state of weak homogeneous turbulence (hereafter denoted HTC for "homogeneous turbulent convection") is favored when the stabilizing effect of the compositional gradient is strong and the destabilizing effect of the thermal gradient is weak (i.e., when the inverse density ratio R_0^{-1}, defined below, is relatively large). Layered convection is favored when the opposite conditions apply.

The efficiency of the convection in transporting heat down the thermal gradient is measured by the Nusselt number, defined as the ratio of the total (diffusive plus dynamical) sensible heat flux to that carried by diffusion alone (where in this case, the diffusion of heat is dominated by radiative transport). The numerical experiments of Rosenblum et al. (2011), Mirouh et al., (2012), and Wood et al., (2013) show that it takes on significantly different values for the two forms of diffusive convection. During HTC it tends to remain small, especially for larger R_0^{-1}, with the total flux being only slightly greater than that carried by diffusion alone. In contrast, Nusselt numbers of ~10–100 typically occur during layered convection. A layer undergoing HTC therefore has the potential to be an effective thermal insulator between convectively mixed regions whereas a layer undergoing layered convection does not. Hence it is important to understand the conditions under which layered convection would develop in the evolving water condensation zone.

In the slow-precipitation limit the condensed particles remain suspended for a time that is long compared to the growth time of the diffusive-convective instability; referring to Fig. 3, we see that this corresponds to a few buoyancy periods. In this regime a fluid parcel is taken to remain saturated as it moves and experiences latent heating/cooling due to condensation/evaporation, but its mass does not change as the water converts between phases. As noted previously, this requires that there is enough *total* water initially to ensure that the condensate mass mixing ratio l always remains positive during the motion. However, for small-amplitude motions, this does not require a significant initial abundance of condensate.

To examine the conditions that would favor layered convection over weak HTC in a saturated layer, we extend the mean-field (γ-instability) theory for layer development to include the effects of condensation. In the theory, layered convection is regarded as a secondary instability that arises under certain conditions from a system undergoing HTC. The instabilities correspond to the unstable growth of perturbations possessing horizontal scales that are much larger than the size of the turbulent eddies. This theory was initially proposed by Radko (2003) to explain layer formation in the fingering convection regime in the ocean; Rosenblum et al. (2011) and Mirouh et al. (2012) later adapted it to successfully explain the results of their numerical simulations of convection and layer formation in the diffusive regime.

To explore layer formation, we adopt an approach that is very similar to that of Rosenblum et al. (2011) and Mirouh et al. (2012). Following in their footsteps, we make use of the Boussinesq approximation (Spiegel and Veronis 1960; Tritton 1977), which allows considerable simplification of the full Eqs. (1a–1f). Certain conditions must be satisfied for this approximation to be applicable. First, the vertical length scale characterizing the dynamics, L_z, must be small in comparison to the pressure scale height and the scale height associated with the adiabatic temperature, that is, $L_z \ll H_0$ and $\Gamma_d L_z / T_0 \ll 1$, respectively. (It should be mentioned that an additional, generally more severe, criterion must

also be satisfied, which is that L_z also be much smaller than the scale height associated with the superadiabatic gradient [e.g., Tritton 1977]. Fortunately, this criterion can be dispensed with by formulating the equations in terms of the potential temperature $T_p = T + \Gamma_d z$. It is therefore essential in general to cast the linearized Boussinesq equations for the perturbation fields in terms of T_p. In the treatment below, however, we solve only for instability in the horizontally-averaged mean-field temperature in a system where the horizontal average of the vertical motion field, w, vanishes. The difference between T_p and T then becomes irrelevant because the vertical advection term associated with the adiabatic lapse rate, $w\Gamma_d z$, vanishes when horizontal averages are taken.) In their numerical study of dry diffusive convection, Rosenblum et al. (2011) found that when conditions favor layer formation, the initial layer thickness is of order 50 times the thermal length scale, which in the present context is given roughly by $(\mathrm{Pr}\,\kappa_r^2 C_p T_0/g^2)^{1/4}$. For typical conditions of interest here, the implied layer thickness, and thus L_z, is then of order of a few meters, far smaller than the pressure or adiabatic temperature scale heights. Thus in this context adopting the Boussinesq approximation appears to be appropriate. This assumes, however, that L_z for a diffusively convecting system with condensation will follow a similar law. One may surmise this will be the case when the density variations associated with the condensation and latent heat release are no larger than those caused by the temperature variations engendered by advection of the background superadiabatic temperature gradient. We are not aware of any results from laboratory or numerical experiments that support or refute this assumption. For the present, we assume that a transition from HTC to layered convection in a condensing system would occur in a manner similar to that seen in dry diffusive convection, pending numerical or experimental evidence to the contrary, and that the ratio of L_z to the scale heights is still small.

In addition to the above conditions, the Boussinesq approximation requires that the physical properties of the fluid, including the dynamic viscosity, radiative conductivity, specific heat, and binary collision coefficient of water in hydrogen-helium be approximately constant over the domain. We also assume that the latent heat of vaporization of water is approximately constant. For typical conditions in the deep atmospheres of the ice giants, we estimate the fractional variation of the latent heat to be ~15% over a pressure scale height, indicating this approximation is reasonable. Finally, because L_z is small, we ignore the variation of the temperature gradient across the layer, that is, we take $\partial^2 T_0/\partial z^2 = 0$ in the following analysis except where it must be retained in the heat balance describing the background, statistically steady HTC state.

We will not present the full form of the Boussinesq equations here; they can be found in Spiegel and Veronis (1960), Mirouh et al. (2012) in the double-diffusive context, and in several texts (Tritton 1977 in particular provides a thorough discussion of their applicability). The γ-instability theory proceeds by ignoring the momentum equations while considering the evolution of the thermal and compositional fields. The equations governing these fields are averaged over small length scales and short time scales to produce the mean-field equations. These are then linearized about an initial background state undergoing HTC diffusive convection to model the time evolution of normal mode perturbations that are uniform in the horizontal and oscillatory in the vertical. The perturbation temperature and composition (specific humidity) fields are divided into the horizontally large-scale components T_1, q_1 and small-scale turbulent components T', q', which are then superimposed on the temperature and humidity fields associated with the homogeneously turbulent basic state to obtain the total fields. The horizontally averaged temperature and humidity fields are given by

$$\langle T\rangle = T_0 + T_1\ ;\ \langle q\rangle = q_0 + q_1, \tag{5}$$

where $T_0(z)$ and $q_0(z)$ are the horizontally and statistically averaged temperature and humidity fields of the HTC basic state and the angle brackets denote horizontal averaging. Horizontal averaging of the Boussinesq temperature and humidity equations yields the following equations for the mean-field perturbations T_1 and q_1:

$$\frac{\partial T_1}{\partial t} + \frac{\partial F_T}{\partial z} = -\frac{T_0}{\epsilon(1-q-l)}\langle E - C\rangle \tag{6a}$$

$$\frac{\partial q_1}{\partial t} + \frac{\partial F_q}{\partial z} = \langle E - C\rangle \tag{6b}$$

where $\epsilon \equiv C_p T_0/L$ and the horizontally averaged thermal and compositional fluxes are given by

$$F_T = \left\langle w'T'\right\rangle - \kappa_r\frac{\partial T_1}{\partial z} - \kappa_r\frac{\partial T_0}{\partial z} \tag{7a}$$

$$F_q = \left\langle w'q'\right\rangle - D_q\frac{\partial q_1}{\partial z} - D_q\frac{\partial q_0}{\partial z} \tag{7b}$$

Eqs (6) and (7) are essentially the dimensional forms of the temperature and composition equations used by Rosenblum et al. (2011) and Mirouh et al. (2012), but now condensation and evaporation lead to the appearance of source terms. In addition, we use specific humidity rather than mean molecular weight for our composition variable.

A fully comprehensive study of layer formation in a diffusively convecting system involving condensation must necessarily consider details of the microphysics of the condensates in conjunction with the dynamics and mass transport in the fluid. Such a study is beyond the scope of this paper. We instead focus on layer formation in the slow-precipitation limit, in which we assume the system is maintained in a saturated state such that the basic state specific humidity $q_0(z)$ follows the saturation profile and, in addition, that the specific humidity perturbations adjust rapidly to the temperature perturbations such that the vapor and condensate remain in a state of saturation equilibrium. We also ignore the effect of pressure perturbations on the saturation specific humidity. This is justified in part by noting that the ratio of the pressure to thermal effect on the saturation specific humidity is

$$\beta/\epsilon\gamma = P(\partial q_s/\partial P)_T/T(\partial q_s/\partial T)_P \sim (L/R_w T)^{-1}.$$

This is derived by recognizing that $\beta \approx -q_s$ when the saturation vapor pressure is small with respect to the total pressure (see Appendix A). The ratio $L/R_w T_0$ is approximately 10 or greater in the deep atmospheres of the ice giants. In addition, the fractional pressure perturbations induced by the motion are a factor of L_z/H_0 smaller than the fractional temperature perturbations; recall $L_z/H_0 \ll 1$ is required for the Boussinesq equations to be applicable (Spiegel and Veronis 1960). Moreover, we deduce that the variation of the background mean saturation humidity with height is dominated by the effect of the background temperature gradient, since the ratio of its effect to that of the mean pressure gradient is of order $L/R_w T_0$. The assumption of saturation quasi-equilibrium then implies

$$\left(q_1, q'\right) \approx \frac{\epsilon\gamma}{T_0}\left(T_1, T'\right). \tag{8}$$

Substituting for $\langle E - C\rangle$ in (6a) from (6b), and using (7a), (7b), and (8), the equation for the time evolution of the large-scale temperature perturbation becomes

$$\begin{aligned}\left(1+\gamma'\right)&\left\{\frac{\partial T_1}{\partial t} + \frac{\partial}{\partial z}\langle w'T'\rangle\right\}\\ &= \left(1+\gamma'\tau\right)\kappa_r\frac{\partial^2 T_1}{\partial z^2} - \gamma'\frac{\partial \ln(Q/T_0)}{\partial z}\left\{< w'T' > -\tau\kappa_r\frac{\partial T_1}{\partial z}\right\}\\ &\quad + \left(1+\gamma'\tau\right)\kappa_r\frac{\partial^2 T_0}{\partial z^2} + \gamma'\frac{\partial \ln(Q/T_0)}{\partial z}\tau\kappa_r\frac{\partial T_0}{\partial z}\end{aligned} \tag{9}$$

where $\tau = D_q/\kappa_r$ is the diffusivity ratio and $\gamma' = \gamma/(1 - q_s - l)$. We have also introduced $Q \equiv \epsilon\gamma = T(\partial q_s/\partial T)_P$ to simplify the notation. Eq. (9) relates the rate of change of the horizontal-average perturbation temperature to the convergence of the vertical turbulent heat flux, average latent heating, and thermal diffusion. In deriving (9), terms proportional to the inverse density scale height have been ignored in comparison to the height derivatives, in accordance with the assumptions associated with making the Boussinesq approximation, but the effect of the scale height $[\partial \ln(Q/T_0)/\partial z]^{-1}$ associated with the saturation humidity has been retained because it is of the same order as the temperature scale height, which can be significantly smaller than the pressure and density scale heights.

Similarly, the heat balance of the statistically steady background HTC state is described by

$$\left(1+\gamma'\right)\frac{\partial}{\partial z}\left\langle w'T'_0\right\rangle = \left(1+\gamma'\tau\right)\kappa_r\frac{\partial^2 T_0}{\partial z^2} - \gamma'\frac{\partial \ln(Q/T_0)}{\partial z}\left\{\left\langle w'T'_0\right\rangle - \tau\kappa_r\frac{\partial T_0}{\partial z}\right\} \tag{10}$$

where again the zero subscript refers to the background HTC state. Subtracting (10) from (9) we obtain

$$\frac{\partial T_1}{\partial t} + \left\{\frac{\partial}{\partial z} + \frac{\gamma'}{1+\gamma'}\frac{\partial \ln(Q/T_0)}{\partial z}\right\}\left[\left\langle w'T'\right\rangle - \left\langle w'T'\right\rangle_0\right] = \frac{\left(1+\gamma'\tau\right)}{1+\gamma'}\kappa_r\frac{\partial^2 T_1}{\partial z^2} + \frac{\gamma'}{1+\gamma'}\frac{\partial \ln(Q/T_0)}{\partial z}\tau\kappa_r\frac{\partial T_1}{\partial z} \tag{11}$$

This equation expresses the evolution of the mean-field temperature perturbation in terms of the excess sensible and latent diffusive and turbulent heat fluxes it produces relative to those of the steady HTC state.

The γ-instability theory proceeds by introducing the thermal Nusselt number Nu_T to relate *local* turbulent thermal fluxes to *local* diffusive fluxes,

$$\mathrm{Nu}_T = \frac{-\kappa_r(\partial T/\partial z) + \langle w'T'\rangle}{-\kappa_r\partial T/\partial z} = 1 - \frac{\langle w'T'\rangle}{\kappa_r\partial T/\partial z} \tag{12}$$

eventually allowing (11) to be expressed entirely in terms of T_1. Using (12) to eliminate the turbulent heat fluxes, that is,

$$\left\langle w'T'\right\rangle = -\kappa_r(\partial\langle T\rangle/\partial z)(\mathrm{Nu}_T - 1)$$

$$\left\langle w'T'\right\rangle_0 = -\kappa_r(\partial T_0/\partial z)(\mathrm{Nu}_0 - 1)$$

with $\langle T\rangle$ given by (5), we find, retaining terms up to first order in the perturbation T_1,

$$\left\langle w'T'\right\rangle - \left\langle w'T'\right\rangle_0 = -\kappa_r\frac{\partial T_0}{\partial z}(\mathrm{Nu}_T - \mathrm{Nu}_0) - \kappa_r\frac{\partial T_1}{\partial z}(\mathrm{Nu}_0 - 1) \tag{13}$$

In (13), Nu_T accounts for the departure from Nu_0 engendered by the perturbations.

At this point it is necessary to introduce the concept of the inverse density ratio (IDR), R_0^{-1}. Mirouh et al. (2012) have given a full account of the significance of this parameter in the problem of dry diffusive convection. As in the dry case, our R_0^{-1} must measure the relative importance of the stabilizing compositional gradient to the destabilizing thermal gradient. However, due to the contribution to the density from the suspended condensate particles, the compositional gradient in this limit is no longer given simply in terms of the mean molecular weight gradient in the gas, as it is in the dry case. Consequently, the definition of R_0^{-1} must be modified for the slow-precipitation ($f_c = 0$) limit. We define R_0^{-1} as follows:

$$R_0^{-1} = -d_q\frac{\partial q_s}{\partial z}\Big/\frac{1}{T_0}\left(\frac{\partial T_0}{\partial z} + \Gamma_s\right) \tag{14}$$

Here we have introduced $d_q \equiv (1/\rho)(\partial\rho/\partial q)_{P,T}$, which expresses the fractional change in density due to a change in the saturation specific humidity. Eq. (1f) for the case $f_c = 0$ shows that

$$d_q = -\frac{1+\xi}{1+\xi q_s - l}$$

It is worth noting that d_q is always negative, and that R_0^{-1} is always positive for a lapse rate that is superadiabatic with respect to the moist adiabat. The definition of R_0^{-1} in (14) arises naturally from non-dimensionalization of the Boussinesq form of the equations (when couched in terms of the potential temperature), using dimensional scaling parameters very similar to those used by Mirouh et al. (2012). Specifically, we may define a characteristic length scale d_* and time scale $t_* = d_*^2/\kappa_r$. The unit of temperature is taken to be $T_* = |\partial T_0/\partial z + \Gamma_s|d_*$, which differs from that used by Mirouh et al. (2012) by the substitution of Γ_s for Γ_d. We additionally introduce a scaling parameter for the specific humidity, $q_* = \kappa_r\nu/(|d_q|gd_*^3)$. Finally, $d_*^4 = \kappa_r\nu T_0/(g|\partial T_0/\partial z + \Gamma_s|)$. With this scaling, the non-dimensional form of our Boussinesq equations becomes isomorphic to the non-dimensional equations for dry diffusive convection presented in Mirouh et al. (2012), apart from the appearance of the source terms related to condensation and evaporation and the appearance of a non-dimensional specific humidity that takes over the role played by the non-dimensional molecular weight in Mirouh et al. (2012). In particular, R_0^{-1} takes on the definition given in (14).

In the standard γ-instability theory for dry diffusive convection, it is assumed that the Nusselt number depends only on the local IDR, Prandtl number, and τ. The inclusion of condensation introduces one additional independent, non-dimensional parameter, related to the latent heat of vaporization of water. In (1e), it appears in the form $\epsilon^{-1} = L/C_pT$. This non-dimensionalization is not unique, however, and we will find it convenient to use Q as our non-dimensional measure of the latent heat. This parameter is given by

$$Q = T(\partial q_s/\partial T)_P = q_s\frac{T}{e_s}\frac{de_s}{dT}\frac{1+\xi q_s - l}{1 - q_s - l}$$

where $e_s(T)$ is the saturation vapor pressure of water. This expression for Q is strictly valid only when the system moves along the water phase equilibrium curve, such that $dl = -dq_s$, which we have been assuming is the case in the slow precipitation limit. To a very good approximation for water in hydrogen atmospheres, the ratio $(1+\xi q_s - l)/(1 - q_s - l)$ remains very close to unity. We can thus take $Q \approx q_sL/R_wT$, since $(T/e_s)(de_s/dT) = L/R_wT$.

An appropriate extension of the γ-instability theory to a condensing system must include the Nusselt number's dependence on Q. We then have $\mathrm{Nu}_T = \mathrm{Nu}_T(R_\rho^{-1},\ Q,\ \tau,\ \mathrm{Pr})$, where R_ρ^{-1} denotes the local IDR that develops in the presence of the mean-field temperature perturbation. Only R_ρ^{-1} and Q vary with altitude after introduction of the perturbation; Pr and τ remain fixed.

Eq. (14) expresses the IDR in terms of R_0^{-1}, the value associated with the basic HTC state. We take this state to also be characterized by $\mathrm{Nu}_0 = \mathrm{Nu}_T(R_0^{-1},\ Q_0)$. (Henceforth we suppress the dependence of Nu_T on the constants Pr and τ). The onset of perturbations in the large-scale temperature and humidity fields causes the local IDR and Nusselt number to vary with height, and this variation must be taken into account in constructing the equations that govern their time evolution. In a saturated system, the local IDR of the perturbed system is

$$R_\rho^{-1} = -d_qQ\frac{\partial\langle T\rangle}{\partial z}\Big/\left(\frac{\partial\langle T\rangle}{\partial z} + \Gamma_s\right) \tag{15}$$

Using (5) to expand $\langle T\rangle$, we obtain, to first order in the perturbation T_1,

$$R_\rho^{-1} = R_0^{-1} - d_q Q_0 \frac{(\partial T_1/\partial z)}{\left(\frac{\partial T_0}{\partial z}+\Gamma_s\right)} - R_0^{-1}\frac{\partial T_1/\partial z}{\left(\frac{\partial T_0}{\partial z}+\Gamma_s\right)} + R_0^{-1}\left\{\frac{L}{R_w T_0} - 1 + \left(\frac{\Gamma_{s0}}{\partial T_0/\partial z + \Gamma_{s0}}\right)\frac{\gamma'}{1+\gamma'}\left(\frac{L}{R_w T_0}-2\right)\right\}\frac{T_1}{T_0} \tag{16}$$

In deriving (16), we have made use of the useful formulas

$$\frac{\partial Q_0}{\partial z} \approx Q_0 \frac{1}{T_0}\frac{\partial T_0}{\partial z}\left(\frac{L}{R_w T_0}-1\right)$$

$$\frac{\partial \Gamma_{s0}}{\partial z} \approx -\Gamma_{s0}\frac{1}{T_0}\frac{\partial T_0}{\partial z}\frac{\gamma'}{1+\gamma'}\left(\frac{L}{R_w T_0}-2\right)$$

where these formulae are based on the approximation $Q \approx q_s L/R_w T_0$. Comparing (16) to the expression for the local IDR derived for dry diffusive convection by Mirouh et al. (2012), we see that each of the first three terms on the right side of (16) has a counterpart appearing in their Eq. (17). For example, the second term on the right in (16) corresponds to the contribution from the perturbed mean molecular weight gradient imparted by the perturbation temperature, and a similar term (albeit unrelated to condensation) appears in Eq. (17) of Mirouh et al. (2012). The last term in (16) appears strictly because of condensation; the first term inside the brackets accounts for the effect of T_1 on Q and the second one accounts for its effect on the local moist adiabatic lapse rate Γ_s (see Appendix A; the sensitivity to temperature occurs through the parameter $\gamma = Q/\epsilon$). Note also that $dl = -dq_s$ has been assumed, as required in the slow-precipitation limit.

The small perturbation temperature T_1 causes Nu_T to be perturbed from Nu_0. Expanding Nu_T in a Taylor series about Nu_0 and retaining terms up to first order, we have

$$\mathrm{Nu}_T \approx \mathrm{Nu}_0 + \left.\frac{\partial \mathrm{Nu}_T}{\partial R_\rho^{-1}}\right]_Q \left(R_\rho^{-1} - R_0^{-1}\right) + \left.\frac{\partial \mathrm{Nu}_T}{\partial Q}\right]_{R_\rho^{-1}} (Q - Q_0) \tag{17}$$

In addition, again using the approximation $Q \approx q_s L/R_w T_0$,

$$Q(T_0+T_1) \approx Q_0 + Q_0\left(\frac{L}{R_w T_0}-1\right)\frac{T_1}{T_0} \tag{18}$$

We now substitute for R_ρ^{-1} in (17) using (16) and for Q using (18), eliminate Nu_T in (13) using (17), and substitute for the turbulent heat fluxes in (11) using (13), to obtain an equation for $\partial T_1/\partial t$:

$$\frac{\partial T_1}{\partial t} = \kappa_r\left\{A_1\frac{\partial^2 T_1}{\partial z^2} + Z_1\frac{\partial T_1}{\partial z} + A_2 T_1\right\} + \frac{(1+\gamma'\tau)}{1+\gamma'}\kappa_r\frac{\partial^2 T_1}{\partial z^2} \tag{19}$$

where

$$A_1 = -\mathrm{Nu}_{,R}\frac{\theta_0}{1-\theta_0}R_0^{-1} + (\mathrm{Nu}_0 - 1)$$

$$A_2 = \mathrm{Nu}_{,R}\frac{\partial T_0}{\partial z}\left(\frac{\partial}{\partial z} + \frac{\gamma'}{1+\gamma'}\frac{\partial \ln(Q_0/T_0)}{\partial z}\right)\left\{\frac{R_0^{-1}}{T_0}\left[\frac{L}{R_w T_0} - 1 + \left(\frac{\Gamma_{s0}}{\partial T_0/\partial z + \Gamma_{s0}}\right)\frac{\gamma'}{1+\gamma'}\left(\frac{L}{R_w T_0}-2\right)\right]\right\} + \mathrm{Nu}_{,Q}\frac{\partial T_0}{\partial z}\left\{\frac{\partial}{\partial z}\left[\frac{Q_0}{T_0}\left(\frac{L}{R_w T_0}-1\right)\right] + \frac{\gamma'}{1+\gamma'}\frac{\partial (Q_0/T_0)}{\partial z}\left(\frac{L}{R_w T_0}-1\right)\right\} \tag{20}$$

Here $\theta_0 = \Gamma_s/|\partial T_0/\partial z|$ is a measure of the superadiabaticity of the layer and satisfies $0 < \theta_0 < 1$. (Recall that for this problem $\partial T_0/\partial z$ is negative). We have also introduced $\mathrm{Nu}_{,R} \equiv \left.\frac{\partial \mathrm{Nu}_T}{\partial R_\rho^{-1}}\right]_Q$ and $\mathrm{Nu}_{,Q} \equiv \left.\frac{\partial \mathrm{Nu}_T}{\partial Q}\right]_{R_\rho^{-1}}$ to simplify notation. We leave Z_1, the coefficient of $\partial T_1/\partial z$ in (19), unspecified for reasons that will soon become clear. In deriving (19) and (20) we have again assumed that $\partial T_0/\partial z$ is approximately constant over the shallow depth L_z of the motion such that terms proportional to $\partial^2 T_0/\partial z^2$ can be ignored.

We are now in position to examine the conditions under which this system will be unstable to formation of a staircase pattern of vertically stacked layers. We look for normal-mode solutions of (19) of the form $\tilde{T}_1 e^{\Lambda t + ikz}$ and obtain the following equation for Λ:

$$\Lambda = \kappa_r\left[-k^2 A_1 + ikZ_1 + A_2 - k^2\frac{(1+\gamma'\tau)}{1+\gamma'}\right] \tag{21}$$

The system will be stable to the development of layers if the real part of Λ is negative. From (21) we see that this will always be the case when A_1 is positive and A_2 is negative (γ' and τ are positive). We also see that the value of Z_1 is irrelevant to the question of stability since ikZ_1 makes no contribution to the real part of Λ.

We first consider the sign of A_1. From (20) it is clear that $A_1 > 0$ if $\mathrm{Nu}_{,R} < 0$, since $\theta_0 < 1$, $\mathrm{Nu}_0 > 1$, and R_0^{-1} is positive. The numerical results of Mirouh et al. (2012) for dry diffusive convection indicate that Nu_T decreases with increasing R_0^{-1}. This is in accord with expectation, since an increase in R_0^{-1} reflects an enhancement in the stabilizing effect of the background compositional gradient over the destabilizing effect of the temperature gradient, resulting in less vigorous diffusive convection and a reduction in the turbulent heat flux.

A physical argument can be made that the same behavior will be encountered in a saturated layer. If, for example, we imagine reducing the superadiabaticity of the layer (i.e. increasing θ_0), then (15) shows that R_0^{-1} increases. However, a reduction in the superadiabaticity of the environment leads to a reduction in the level of the diffusive cooling that is the source of the overdamping driving the diffusive convection. As a result, the diffusive convection becomes less vigorous and the associated heat flux and Nu_T decrease. Consequently, a reduction in the superadiabaticity leads to an increase in R_0^{-1} and decrease in Nu_T. These changes occur with opposite sign if the superadiabaticity is increased. We conclude that $\mathrm{Nu}_{,R}$ is negative and A_1 is positive.

Although the expression for A_2 in (20) is considerably more complicated, it is nevertheless straightforward to evaluate the sign of the first term (proportional to $\mathrm{Nu}_{,R}$). We introduce the following variables:

$$y = \frac{L}{R_w T_0}$$

$$\chi = \frac{\gamma'}{1+\gamma'}\left(\frac{\Gamma_{s0}}{\partial T_0/\partial z + \Gamma_{s0}}\right)$$

Since we are interested only in lapse rates that are superadiabatic with respect to the moist adiabat, the relevant domain of χ is $(-\infty, 0^-)$. In terms of these variables the first term of A_2 becomes

$$\mathrm{Nu}_{,R}\left(\frac{1}{T_0}\frac{\partial T_0}{\partial z}\right)^2 R_0^{-1}(y-2)\left\{\frac{1+2\gamma'}{1+\gamma'}(y-1) - \frac{y}{y-2} + \chi\left[\frac{3+2\gamma'}{1+\gamma'}y - \frac{5+3\gamma'}{1+\gamma'} - \frac{y}{y-2}\right] + 2\chi^2(y-2)\right\} \tag{22}$$

In deriving this expression, and in the analysis that follows, d_q is treated as approximately constant, which is necessary to maintain consistency with the approximations $Q \approx q_s L/R_w T_0$ and $dl = -dq_s$. Typical values for y and γ' for water in the ice giants, at a level where the temperature is ~ 450 K, are $y \approx 10$ and $\gamma' \approx 2$. For

these values, the term inside the curly brackets in (22) is positive for all χ. Consequently, the sign of the expression in (22) is the same as that of $\mathrm{Nu}_{,R}$, which we have concluded is negative.

It is worth noting that the result for the sign of (22) hinges to some extent on y being relatively large. For example, if we were considering a condensable gas with the same properties as water but with only 30% of its latent heat of vaporization L, then the term in brackets would become negative. However, such low values for y do not appear to be relevant at the condensation level for any time during the cooling histories of the ice giants.

It remains to determine the sign of the term proportional to $\mathrm{Nu}_{,Q}$ in (20). In terms of the parameter y defined above, this term can be re-written

$$\mathrm{Nu}_{,Q}\left(\frac{1}{T_0}\frac{\partial T_0}{\partial z}\right)^2 Q_0\left\{\frac{1+2\gamma'}{1+\gamma'}(y-1)(y-2)-y\right\} \tag{23}$$

The term in brackets is positive for all values of y and γ' in the range of interest, and therefore the sign of (23) will be the same as that of $\mathrm{Nu}_{,Q}$.

$\mathrm{Nu}_{,Q}$ represents the change in the local Nusselt number engendered by a small change in Q, with all other parameters held fixed, *including* R_0^{-1}. Our physical intuition suggests $\mathrm{Nu}_{,Q}$ is negative, according to the following argument. Consider two diffusively convecting systems undergoing HTC that are nearly identical and that carry the same total (sensible plus latent) heat flux and possess the same value of R_0^{-1} at a level where the temperature in the two saturated systems is equal. It is necessary to choose R_0^{-1} to be the same for both systems because we are interested in assessing the sign of $\mathrm{Nu}_{,Q}$ for fixed R_0^{-1}. Now imagine that the latent heat of vaporization of the vapor in one of the systems is slightly larger than that of the other, implying a larger value of Q_0 at the level where the temperatures are equal. By (15), since R_0^{-1} is being held fixed, the superadiabatic lapse rate must be larger in the system with larger Q_0 (this is in fact true only for lapse rates greater than a critical value; see the discussion following Eq. [33] below). The larger lapse rate increases the thermal diffusion; in addition, the sensible and latent turbulent heat fluxes increase as well. However, given that we are considering the *total* heat flux in the two systems to be the same, the increase in the latent heat flux in the system with larger Q_0 must to some extent buffer the increase in the sensible turbulent heat flux, such that the increase in the latter is less than it would need to be to keep the local Nusselt number unchanged. Consequently, $\mathrm{Nu}_T - 1$, which is defined as the ratio of the total *sensible* turbulent heat flux to that of the diffusive heat flux, decreases (see Eq. 12). According to this argument, $\mathrm{Nu}_{,Q}$ should be negative.

It is possible to place this argument on a more quantitative footing for a saturated system in the slow-precipitation limit. The inverse flux ratio γ_{tot}^{-1}, defined as the ratio of the compositional buoyancy flux to the thermal buoyancy flux, is given by

$$\gamma_{tot}^{-1} = \frac{T_0\left(\langle w'q'\rangle - D_q\partial q/\partial z\right)}{\left(\langle w'T'\rangle - \kappa_r\partial T/\partial z\right)} \tag{24}$$

(Rosenblum et al., 2011; Mirouh et al., 2012). (Note that γ_{tot}^{-1} should not to be confused with the parameters γ or γ' defined previously; we have chosen to use this notation to maintain continuity with that used by Rosenblum et al. and Mirouh et al.) Using (8) and the definition of Nu_T in (12), we find a simple relation exists between γ_{tot}^{-1} and Nu_T in a saturated system:

$$\gamma_{tot}^{-1} = Q\left(1-\frac{1-\tau}{\mathrm{Nu}_T}\right) \tag{25}$$

This relationship tying γ_{tot}^{-1} to Nu_T is peculiar to a system in which the vapor and condensate are always in phase equilibrium; in a non-condensing system, the two parameters are independent of one another.

Using (12), (24) and the definition of y given above, the total (sensible plus latent heat) flux in the system can be written

$$F_{tot}/\rho_0 C_p = -\kappa_r\frac{\partial T}{\partial z}\mathrm{Nu}_T\left(1+\frac{R_w y}{C_p}\gamma_{tot}^{-1}\right) \tag{26}$$

We wish to determine the sign of $\mathrm{Nu}_{,Q}$ for the HTC state under conditions where F_{tot} and R_0^{-1} are held fixed. Taking the derivative of $\ln(F_{tot}/\rho_0 C_p)$ in (26) with respect to y and setting it to zero, we obtain

$$\frac{\partial}{\partial y}\ln\frac{\partial T_0}{\partial z}+\frac{1}{\mathrm{Nu}}\frac{\partial \mathrm{Nu}}{\partial y}+\frac{1}{1+\frac{R_w y}{C_p}\gamma_{tot}^{-1}}\left[\frac{R_w}{C_p}\gamma_{tot}^{-1}+\frac{R_w}{C_p}y\frac{\partial\gamma_{tot}^{-1}}{\partial y}\right]=0 \tag{27}$$

All derivatives are evaluated holding R_0^{-1} constant. Next, we evaluate $\partial\gamma_{tot}^{-1}/\partial y$ using (25),

$$\frac{\partial\gamma_{tot}^{-1}}{\partial y}=\frac{\partial Q_0}{\partial y}\left(1-\frac{1-\tau}{\mathrm{Nu}}\right)+\frac{Q_0(1-\tau)}{\mathrm{Nu}^2}\frac{\partial \mathrm{Nu}}{\partial y} \tag{28}$$

substitute (28) into (27), multiply both sides by $\partial y/\partial Q_0$, and gather like terms. We find

$$-\frac{\partial y}{\partial Q_0}\frac{\partial}{\partial y}\ln\frac{\partial T_0}{\partial z}=\frac{1}{\mathrm{Nu}}\frac{\partial \mathrm{Nu}}{\partial Q_0}\left[1+\frac{\frac{R_w}{C_p}yQ_0(1-\tau)}{\mathrm{Nu}\left(1+\frac{R_w y}{C_p}\gamma_{tot}^{-1}\right)}\right]$$
$$+\frac{1-\frac{1-\tau}{\mathrm{Nu}}}{1+\frac{R_w y}{C_p}\gamma_{tot}^{-1}}\left\{\frac{R_w}{C_p}Q_0\frac{\partial y}{\partial Q_0}+\frac{R_w}{C_p}y\right\} \tag{29}$$

where we have again used (25) to simplify the last term. Since

$$\frac{\partial y}{\partial Q_0}=-\frac{y}{Q_0(y-1)}$$

the last term in brackets in (29) can be re-written:

$$\frac{R_w}{C_p}Q_0\frac{\partial y}{\partial Q_0}+\frac{R_w}{C_p}y=\frac{R_w}{C_p}y\left(\frac{y-2}{y-1}\right) \tag{30}$$

Finally, we must evaluate $\frac{\partial}{\partial y}\ln\frac{\partial T_0}{\partial z}$ for fixed R_0^{-1}. We accomplish this by taking the derivative of R_0^{-1} with respect to y and setting it to zero. Using the formula for $\partial y/\partial Q_0$ given above as well as the formulas for $\partial Q_0/\partial z$ and $\partial\Gamma_{s0}/\partial z$ following (16), we obtain

$$\frac{\partial}{\partial y}\left(\frac{\partial T_0}{\partial z}\right)=\frac{\partial T_0}{\partial z}\left[\frac{\partial T_0/\partial z+\Gamma_s}{\Gamma_s}\left(\frac{y-1}{y}\right)\right]+\frac{\gamma'}{1+\gamma'}\left(\frac{y-2}{y}\right) \tag{31}$$

With (31) in hand, and using (30) and the formula for $\partial y/\partial Q_0$, we can now express our formula for $\mathrm{Nu}_{,Q}$ in a form that allows us to evaluate its sign:

$$\frac{1}{\mathrm{Nu}}\mathrm{Nu}_{,Q}\left[1+\frac{yQ_0(1-\tau)}{\mathrm{Nu}\left(1+\frac{R_w y}{C_p}\gamma_{tot}^{-1}\right)}\right]$$
$$=-\frac{1-\frac{1-\tau}{\mathrm{Nu}}}{1+\frac{R_w y}{C_p}\gamma_{tot}^{-1}}\frac{R_w}{C_p}y\left(\frac{y-2}{y-1}\right)$$
$$+\frac{1}{Q_0}\left(\frac{\theta_0-1}{\theta_0}+\frac{\gamma'}{1+\gamma'}\frac{y-2}{y-1}\right) \tag{32}$$

Here we have used our definition $\theta_0=\Gamma_s/|\partial T_0/\partial z|$, $0<\theta_0<1$. The coefficient of $\mathrm{Nu}_{,Q}$ on the left side of (32) is always positive, since each individual term is positive. The first term on the right side of (32) is always negative, since $\mathrm{Nu}>1$, $\tau\ll 1$, $y\gg 1$, and by (25), $\gamma_{tot}^{-1}>0$. Therefore, $\mathrm{Nu}_{,Q}$ will always be negative if the last term on the right of (32) is negative. This is the case when $\theta_0<\theta_c$, with

$$\theta_c=\left(1+\frac{\gamma'}{1+\gamma'}\frac{y-2}{y-1}\right)^{-1} \tag{33}$$

For typical values $y \approx 10$ and $\gamma' \approx 2$, θ_c is approximately 0.63, meaning that $\mathrm{Nu}_{,Q}$ will always be negative for superadiabatic lapse rates greater than approximately 1.6 Γ_s. The origin of (33) stems from the fact that an increase in Q_0 at fixed R_0^{-1}does not necessarily engender an increase in the lapse rate, contrary to what we surmised above; for smaller lapse rates, a decrease in Γ_s becomes the more important effect in maintaining a constant R_0^{-1}.

It is essential to note, however, that (33) is a sufficient, but not necessary, condition for the suppression of layer formation. In fact, since the first term on the right in (32) is always negative, the actual value of θ_0 for which $\mathrm{Nu}_{,Q}$vanishes is always greater than θ_c by an amount that depends on the specific parameter values. We conclude that in the slow-precipitation limit, $\mathrm{Nu}_{,Q}$ is generally negative for any superadiabatic lapse rate unless it lies close to that of the moist adiabat.

We have shown that, when $\mathrm{Nu}_{,Q}$ is negative, all the terms in the sum on the right side of the expression for A_2 in (20) are negative. In addition, A_2 may be negative even for small positive $\mathrm{Nu}_{,Q}$ if the term proportional to $\mathrm{Nu}_{,R}$ is sufficiently negative. Inspecting (22), and noting that the definition of χ implies $\chi \to -\infty$ as the lapse rate approaches a moist adiabat, suggests the term proportional to $\mathrm{Nu}_{,R}$ will indeed drive A_2 to negative values even for lapse rates near the moist adiabat (that is, for $\theta_0 \approx 1$), but a detailed understanding of this behavior requires the value of $\mathrm{Nu}_{,R}$, which is not available.

It therefore appears that A_2 will generally be negative for all superadiabatic lapse rates, with the possible exception of lapse rates lying very close to the moist adiabat. We have also argued that A_1 must be positive. Consequently, (21) shows that the real part of Λ must be negative. Therefore, we conclude that the system is generally stable to the development of layers in the slow-precipitation limit.

We thus see that a condensation zone undergoing HTC will be stable against forming layers if the turbulent fluid remains saturated. Continued cycling between condensation of vapor and evaporation of suspended particles would be conducive to maintaining saturation. On the other hand, if rainout is too rapid, then the system crosses into the fast precipitation regime, where all forms of diffusive convection are inhibited.

It therefore appears that the range of conditions that would potentially support robust layered convection may be quite limited in scope. Moreover, it is possible that complete saturation may not be required, because layer formation will also be suppressed in an unsaturated zone if the relative humidity is high enough to allow R_0^{-1} to exceed the maximum value required for the γ-instability (i.e., $R_0^{-1} \approx 2$, see Mirouh et al., 2012) and if latent heat effects in this scenario play a secondary role.

In Fig. 4 we summarize our results for the stability of a saturated condensation zone in the fast and slow precipitation limits. For comparison, we also include the results of Rosenblum et al. (2011) and Mirouh et al. (2012) for the case of a compositionally stratified layer in which there is no condensation.

Although layered convection is suppressed under saturated conditions, HTC may be able to operate and in this instance an estimate of the efficiency of heat transfer across the layer is desirable. From (26) we see that the effective Nusselt number for the *total* heat flux across the layer is

$$\mathrm{Nu}_e = \mathrm{Nu}_T\left(1 + \frac{R_w y}{C_p}\gamma_{tot}^{-1}\right)$$

where Nu_T is the ratio of the sensible heat flux to diffusive heat flux in the system. The term in brackets represents the enhancement imparted by latent heat transport. Based on (25), the value of γ_{tot}^{-1} is at most equal to Q, and consequently a typical value for the enhancement is ~3 or less. The numerical studies of dry diffusive convection by Rosenblum et al. (2011) and Mirouh et al. (2012) show that the Nusselt number of a system undergoing HTC is generally quite low, typically less than ~3, especially for the cases characterized by larger R_0^{-1}. If we assume that the advent of condensation in the system does not significantly increase the *sensible* heat flux in the system (as measured by Nu_T) over that of a non-condensing system governed by similar external parameters, then it is clear that the effective Nusselt number of the saturated HTC system will remain relatively low, perhaps of order 10 or less. Given the inherent inefficiency of radiative heat transport across a deep condensation zone, the total heat flux carried across a saturated layer by HTC will therefore likely still be small enough for the layer to act effectively as an insulator during cooling of the planet. However, without the availability of numerical or laboratory experiments to test our assumption, we must regard the efficiency of heat transfer by HTC across a saturated layer in the slow-precipitation limit as an open question.

5. Evolution and erosion of the gradient zone

The results presented above suggest a scenario in which water saturation may have played an important role in the cooling history of the ice giants. A schematic illustration of that role is shown in Fig. 5. As the planet cooled from a hot accretion state, water would eventually become saturated and condense at low pressures. At first, at low pressures, the condensation layer would likely to be too thin, and radiative transport too efficient, for significant suppression of heat transfer to take place. Further cooling of the planet, however, would cause the saturated layer to extend to greater depths and to thicken. If water was sufficiently abundant in the layer, ordinary moist convection would be inhibited and only a combination of radiative diffusion and double-diffusive convection would remain to transport heat. Eventually a significant drop in temperature (in excess of that associated with the moist adiabat) would develop across the layer as it became opaque to radiation at great depths. As shown above, diffusive convection would have been unlikely to significantly mitigate this excess temperature difference.

In the early stages following formation of a robust stable layer, the lapse rate in the layer would be only slightly greater than the local moist adiabat. The total heat flux through the layer, driven by this relatively small gradient, would be too low initially to balance the rate at which energy was emitted to space from the planet's photosphere. Consequently, at this stage the stable layer in essence would have behaved like an insulator, thermally separating the deep atmosphere and interior from the layers above. Since the outer layers had a relatively small effective heat capacity compared to the planet as a whole, they would cool rapidly.

We can estimate a cooling time scale, τ_c, for an adiabatic atmosphere lying above pressure p_c from the formula

$$\tau_c \sim \frac{C_p \Delta\vartheta_0}{F_{int}} \frac{p_0}{(1+\kappa)g}\left\{\left(\frac{p_c}{p_0}\right)^{1+\kappa} - 1\right\} \tag{34}$$

here p_0 is the reference pressure for an adiabat with potential temperature ϑ_0; g is the surface gravity; F_{int} is the internal heat flux; C_p is the specific heat; and κ is the ratio of the gas constant to C_p for a predominantly H_2-He mixture. As an example, we can estimate the time required for Uranus' effective temperature to fall from 70 K to 60 K. We use data from the atmosphere model grids of Fortney et al. (2011) to relate ϑ_0 to the effective temperature at a given epoch. Their model also yields an internal heat flux F_{int} of ~0.08 W m^{-2} for the time when the effective temperature was 60 K (assuming Uranus was at its present distance from the Sun). When the effective temperature is 70 K, the model yields $\vartheta_0 \approx 205$ K, while $\vartheta_0 \approx 155$ K when the effective temperature is 60 K. We therefore take $\Delta\vartheta_0 = 50$ K in Eq. (34). Also, we take $\kappa \approx 0.3$. Assuming a water mole fraction below the condensation zone of

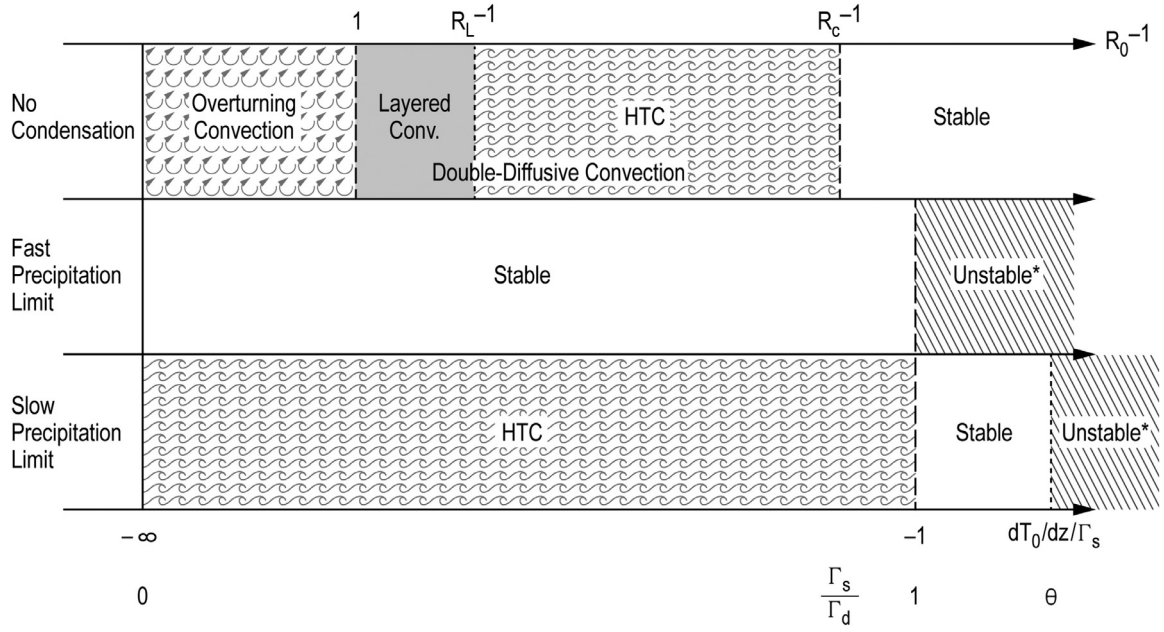

Fig. 4. Stability diagram for the fast and slow precipitation limits. Also shown is the case of compositional stratification without condensation (Rosenblum et al., 2011; Mirouh et al., 2012). Both the ratio of the environmental temperature gradient to the moist adiabat, $(dT_0/dz)/\Gamma_s$, and the parameter $\theta = \Gamma_s/|dT_0/dz|$, are given along the abscissa. "HTC" stands for homogeneous turbulent convection. The inverse density ratio R_0^{-1} for different degrees of stratification is indicated at the top of the diagram. In a non-condensing system, the transition from stability to HTC occurs at $R_c^{-1} = (Pr+1)/(Pr+\tau)$; for the small values of Pr and τ in the ice giants, this is large and the associated neutral lapse rate lies close to the dry adiabat. R_L^{-1} denotes the inverse density ratio at which a non-condensing system transitions from HTC to layered convection. Mirouh et al. (2012) find R_L^{-1} to be typically ~ 2 or less, depending on the values of Pr and τ. The asterisk appearing on the label "Unstable" is meant to remind the reader that these regimes, although unstable, possess sub-adiabatic lapse rates and the ensuing buoyancy-driven motions transport heat downward, causing the lapse rate to relax toward the neutrally stable value. A region where layered convection is favored may exist between the HTC and stable regimes for the slow-precipitation limit; if so, it would be confined to a narrow zone lying very close to the stable boundary.

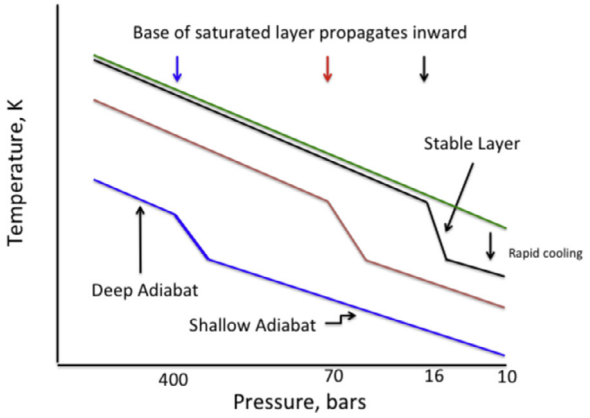

Fig. 5. Schematic diagram showing temperature-pressure profiles at four different epochs during the cooling of an ice giant whose water abundance at depth exceeds the critical value for convective inhibition. Proceeding from the top down, the green profile represents the adiabatic temperature profile at pressures higher than 10 bars just prior to formation of a robust stable saturation layer at shallow levels. The black line represents the profile created just after a phase of rapid cooling of the outer layers following creation of a stable, insulating layer. The red and blue profiles represent later epochs in the thermal evolution during which the planet slowly cools on a billion-year time scale. Note that the stable saturation layer slowly propagates to higher pressures as the planet cools, as indicated by the row of arrows at the top of the diagram. "(For interpretation of the references to color in this figure legend, the reader is referred to the web version of this article.)".

0.03, we expect the base of the saturation layer to lie at $p_c \approx 155$ bars when $\vartheta_0 \approx 205$ K. Putting this information into Eq. (34), we find $\tau_c \leq 7 \times 10^5$ years. This time scale is very short in comparison to the cooling time scale of the interior, which is on the order of 10^9 years.

The above result suggests that the overlying atmosphere, thermally isolated from the interior by the stable layer, may cool rapidly soon after the layer is formed. Above the effective top of the stable layer (which is located somewhere just below the level where $\alpha \approx 0$), convection remains active, driven by the planet's thermal emission. As the outer convective envelope cools, low temperatures radiatively diffuse into the stable layer from above, steepening the local lapse rate and, if saturation is maintained, increasing the local stability. This process continues until the radiative heat flux, driven by the growing superadiabatic temperature gradient, balances the ebbing planetary thermal emission.

Whether this scenario actually happens, however, depends on the ability of the stable layer to resist the erosive effects of the overlying convection for a time that is comparable to or longer than τ_c. The erosion occurs through steady intrusion of the overlying convective layer into the top of the gradient zone as stable fluid is entrained into the mixed layer. The convective mixing at the top of the zone must also be accompanied by precipitation and local drying to be effective; otherwise, the conditions necessary for convective instability will not propagate downward into the stable layer. (This latter point appears to be a special feature of the problem of mixing across a density interface when the stabilizing solute is condensable. Saturation prevents complete mixing of a condensable solute. This is a distinct departure from the usual case of a non-condensing solute, where the final state approached must ultimately be one of uniformly mixed entropy and composition.) The entrainment phenomenon has been studied in the laboratory (Turner 1973; Bergman et al., 1986), but apparently only for non-condensing systems. To make further progress toward estimating the rate of erosion, we will assume that the convective mixing efficiently dries the interfacial region at the top of the gradient zone and that the experimental results for non-condensing systems can be applied. Experiments on salt-stratified systems heated from be-

low (Bergman et al., 1986) indicate that a thin interfacial boundary layer develops between the mixed layer and stable region. The compositional stratification is seen to dominate the net density difference $\Delta\rho$ across the interface; the contribution from the small temperature step is negligible. The entrainment velocity u_e of the mixed layer into the stable region is observed to be given by

$$\frac{u_e}{u_*} = A\ \mathrm{Ri}^{-1} \tag{35a}$$

where u_* is the velocity scale of the convection, $\mathrm{Ri} = g\Delta\rho\delta_b/\rho u_*^2$ is the Richardson number, ρ the density, δ_b is the depth of the mixed layer, and A is a correlation constant. For the salt-stratified system studied by Bergman et al. (1986), $A \approx 0.2$, but in general this constant will depend on Pr and τ. Using the definition of u_* in terms of the convective heat flux F_{int} and depth of the mixed layer (Bergman et al., 1986), Eq. (35a) can be expressed in a more useful form:

$$u_e = A\frac{F_{int}}{\Delta\rho c T} = A\frac{\kappa}{(1-\kappa)}\frac{F}{p\Delta q} \tag{35b}$$

where c is the specific heat at constant volume of the fluid and $\kappa = R/C_p$. The second equality on the right of Eq. (35b) pertains to the planetary case with an interface at pressure p and density jump $\Delta\rho = \rho\Delta q$, where Δq is the drop in specific humidity across the interface. A similar formula can be found by invoking the physical argument that the rate of increase in potential energy due to mixing of stable fluid across the interface cannot exceed the work available from the convection (e.g., Turner 1973). The derivation yields (35b) with $A \approx 2(1-\kappa)$ or ~1.4, but this corresponds to an upper limit in terms of the work available and the convection is very likely to be far less efficient in redistributing the mass. For example, the energy-based calculation ignores the portion of convective work that is lost to radiation of gravity waves excited at the interface and the extra work needed to vertically redistribute any condensed particles that may be present. The dynamics of the erosion of a gradient zone imbedded between convectively mixed layers is of great interest in the design of salt-gradient solar ponds used for collection and storage of solar energy (Nielsen 1979; Sreenivas et al., 1995; Suárez et al., 2010). Field observations of solar ponds have indicated that there may be a regime for sufficiently large salinity gradients (and therefore large R_0^{-1}) in which the gradient zone grows rather than decays during its interaction with the mixed layers (Nielsen 1979; Hull et al., 1989). Unfortunately, the measurements are difficult given the slow rates of interface motion and exposure of the solar ponds to the variations of the outdoor environment. In addition, no model has yet been formulated that satisfactorily accounts for the observations of the equilibrium condition (that is, where growth and erosion just balance) over a large range of density ratio. It must also be kept in mind that the Prandtl number of these salt-gradient systems is at least an order of magnitude larger than that expected for a gradient zone in the ice giants. Consequently, we cannot yet say whether or not gradient zone growth might occur if large mean molecular weight gradients develop in the condensation layer. For the present, we will assume that only erosion of the gradient zone occurs, and that the entrainment rate is given by (35b), while noting that this may in fact underestimate the actual longevity of the stable layer.

Fig. 6 shows the ratio of the time scale for erosion of the gradient zone, τ_e, to the cooling time scale τ_c of the overlying convective envelope (see Eq. (34) as a function of the effective temperature the planet had at different stages in its cooling history. The erosion time scale τ_e was estimated from the time required for the entrainment interface to travel one scale height of the saturated vapor profile, that is, $\tau_e \sim x_v H/u_e$, where H is the local pressure scale height and x_v is a reduction factor that accounts for the initial saturation profile. Over a range of 60 K to 90 K in the effective temperature, x_v varies from about 0.6 to 0.9. The entrainment velocity u_e is taken from (35b) with $A = 0.2$ and $\Delta q \approx q_d/2$, with q_d equal to the water mass mixing ratio in the abyssal atmosphere below the condensation zone.

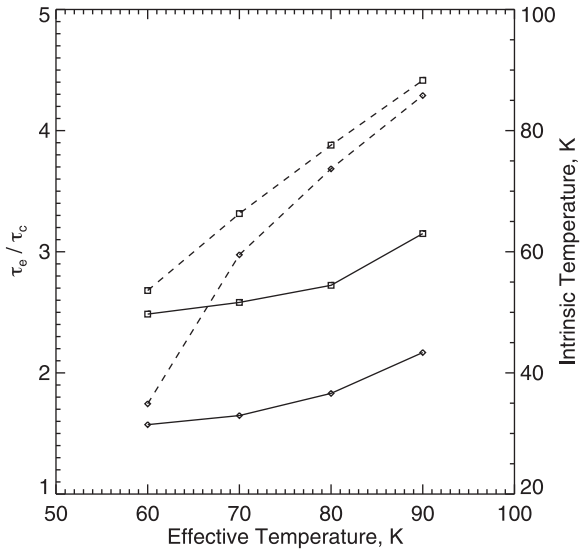

Fig. 6. Solid curves show the ratio of the erosion time scale to the cooling time scale in the ice giants as a function of the effective temperature of the planet. The dashed curves indicate the relationship between the internal heat flux for each planet (expressed in terms of the intrinsic temperature, $F_{int} = \sigma T_i^4$, scale on the right) and its effective temperature, as specified by the atmospheric model grids of Fortney et al. (2011). The curves with diamond symbols are for Uranus and curves with square symbols are for Neptune.

We see in Fig. 6 that in general τ_e is comparable to or greater than τ_c over the range of interest in effective temperature. This suggests that significant cooling of the outer convective envelope may have occurred during the time interval over which the stable gradient zone thinned due to erosion and drying by entrainment. This is an important point, since, if the opposite were true, then water condensation would have had little effect on the thermal evolution of the planet. The system would instead have evolved quickly to a state in which a water-rich deep interior and a dry, convecting outer layer would have been separated by a very thin diffusive interface, across which all the heat flux required to maintain a quasi-steady state would have been driven by a relatively small potential temperature drop.

The results shown in Fig. 6 suggest a different story, however. When $\tau_e > \tau_c$, there is sufficient time to develop a significant temperature drop across the stable zone before a quasi-steady state is established. When the layer is moist enough for α to be sufficiently negative, Nu_0 will be less than ~ 3 and the heat flux across the layer will be (at most) only a small factor greater than that transported by radiative diffusion alone. A quasi-steady layer situated at pressure p and characterized by a radiative diffusivity κ_r will have a depth of $\delta \sim \mathrm{Nu}_0\kappa_r(\Delta T/T)(p/\kappa F_{int})$. To give a numerical example, Uranus' intrinsic temperature was $T_i \sim 59.5$ K (the internal heat flux $F_{int} = \sigma T_i^4$, see Fig. 6) and the temperature at the 10-bar level was ~ 204 K when its effective temperature was $T_{eff} \sim 70$ K, according to the atmospheric grid models of Fortney et al. (2011). This allows us to estimate that the base of the saturation zone would be located near 150 bar for an abyssal water mole fraction of 0.04, the temperature there would be ~ 430 K, and $\alpha \approx -1.4$. Estimation of κ_r is problematic, as it depends on the Rosseland mean opacity χ_{Ros} for these conditions, which we have not attempted to calculate for this study and which in any case is likely to be sensitive to the poorly known abundances of water, methane, and ammonia

at great depths. Guillot et al., (1994) estimated χ_{Ros} for a specific pressure-temperature profile in current-day Uranus; their results (that include the contributions of H_2O, CH_4, and NH_3) suggest that χ_{Ros} ranges between roughly 1 and 30 $cm^2\,g^{-1}$ in the outer convective envelope. For a temperature of $\sim$ 500 K and pressure of $\sim$ 500 bar, their model yields $\chi_{Ros} \sim 5$ $cm^2\,g^{-1}$. Since for the present example we are interested in conditions with a lower pressure (150 bar) but similar temperature, we infer that $\chi_{Ros} < 5$ $cm^2\,g^{-1}$. Using formula (2) from Guillot et al., (1994) to relate κ_r to χ_{Ros}, we obtain $\kappa_r > 0.3$ $cm^2\,s^{-1}$. For a (potential) temperature drop of $\Delta T \sim 50$ K, corresponding to a change of $\sim$ 10 K in T_{eff}, we then estimate δ to be greater than 0.25 km, with this lower bound becoming somewhat larger if Nu_0 is near its maximum value of $\sim$ 3. This implies $\theta \ll 1$ and from (9), $R_0^{-1} \approx 2.4$ in the layer. For this example, the gradient zone is very shallow and significantly superadiabatic. Doing a similar calculation for Uranus with the same water abundance, $T_{eff} \sim 60$ K, and $\chi_{Ros} = 5$ $cm^2\,g^{-1}$ yields $\delta \sim (1.2\,\mathrm{km}) \times Nu_0$, $\alpha \approx -1.1$, and $R_0^{-1} \approx 2.1$. The layer is somewhat thicker (for the same value of χ_{Ros}) largely due to the lower value of T_i (see Fig. 6).

Once a sufficiently steep temperature gradient has formed across the stable layer, the diffusive heat flux through the layer thermally reconnects the deep atmosphere and interior with the atmosphere lying above. The entire atmosphere and interior then continue to cool as a unit, but on a slow, billion-year time scale and on separate adiabats connected across the stable layer by a superadiabatic temperature gradient.

Implicit in the preceding discussion is the assumption that the gradient zone remains saturated (or nearly so) during the cooling process throughout the region that lies below the interface with the mixed layer and above the base of the condensation zone, and that this region therefore remains stable against ordinary convection as a result of a sufficiently negative molecular weight gradient. The time scale for rewetting of the gradient zone through upward diffusion of water from the interior is $\tau_q \sim \delta^2/D_q$. Taking $\delta \sim 1$ km and $D_q \sim 3 \times 10^{-3}$ $cm^2\ s^{-1}$ yields $\tau_q \sim 10^5$ years, which is small compared to the cooling time τ_c. Thus there is ample time for diffusion to re-moisten the gradient zone during the cooling process if rainout is not a dominant factor. The assumption is further supported when it is recalled that the saturated layer is either completely stable or at most undergoes weak homogeneous turbulent convection. Hence the vigorous upwelling associated with strongly precipitating systems would be absent. In a layer stable to ordinary and diffusive convection, radiative and molecular diffusion dominate transport, vertical motions are weak, and little condensation and precipitation can occur. In Section 3 we found that HTC can operate if condensed droplets remain entrained in the motion for several buoyancy periods. Some precipitation could occur in the gentle updrafts of this convection, but the layer would nevertheless remain close to saturation if the droplets evaporate before settling out of the layer.

This being said, it is nevertheless conceivable that a regime may exist in which sustained (but intermittent) HTC would eventually dry the gradient zone enough for it to collapse. It is therefore worthwhile to speculate on what the consequences would be. Clearly, the superadiabatic lapse rate within the zone, no longer stabilized by the compositional gradient, would drive vigorous convection, mixing the formerly stable layer with the overlying envelope. Rapid mixing would initially create a near-stepwise discontinuity in the mean molecular weight and temperature at the new interface between the dry outer envelope and warm, moist interior. The interface would be formally stable to convection if the interior is sufficiently wet, but a large diffusive heat flux, driven by the temperature drop across a shallow boundary layer, could potentially produce catastrophic overturning and mixing of the moist interior with the overlying dry envelope. This could possibly lead to substantial warming of the outer envelope, but it is not clear whether sufficient energy would initially be available to do the work necessary to redistribute the water. In any case, significant re-mixing of the deep water above the condensation level would re-establish a saturated, stable gradient zone and the entire process would repeat. This suggests a picture of episodic cooling of the ice giants, with long periods of steady cooling punctuated by large, sudden bursts of internal heat release. Alternatively, the system could settle into a state with the interior and envelope separated by a stable, diffusive interface. As time proceeds, the temperature interface becomes thicker than the compositional interface due to the larger diffusivity of heat. This eventually produces unstable net density stratification above the water interface. When the depth of this unstable layer reaches a critical value, it detaches from the interface to become a buoyant thermal (Linden and Shirtcliffe 1978; Carpenter et al., 2012). This process would also produce an intermittent source of internal heat for the outer, dry envelope, leading to smaller outbursts of convection and perhaps episodic triggering of upper level cloud formation. Note, however, that if the gradient zone behaved effectively as an insulator for a time of order τ_c before collapsing, then cooling of the overlying envelope during this time could have been significant and largely irreversible. If so, then water condensation would have had a substantial effect on the planet's cooling history.

6. Summary and conclusions

We have shown that condensation of water in the deep atmosphere of the ice giants will inhibit ordinary moist convection within the saturated layer if the water mole fraction beneath the saturation zone exceeds a critical value. Double-diffusive convection is also suppressed when the condensate sedimentation time is short compared to the growth time of the diffusive convective instability. In the opposite limit, the layer can be overstable to homogeneous, turbulent diffusive convection, but layered convection is unlikely to develop. This means that heat is inefficiently transported through the layer either by pure radiative diffusion or by low-Nusselt number diffusive convection. The layer then behaves effectively like an insulator, providing a mechanism for trapping the primordial heat of the planet in the interior. The degree to which its formation affects the planet's thermal history depends on both its ability to resist entrainment into the overlying convective envelope and ability to retain enough water to impart a stable net density stratification. We have already discussed various issues concerning the likelihood that these conditions would be satisfied for an extended period of time, but the overall significance and consequences of entrainment and drying of the layer require further study.

While we have proposed that water condensation may have had an important impact on the thermal trajectory of the ice giants, the results of this work do not provide an immediate explanation for the difference existing between their present-day intrinsic luminosities. If the water abundance in Uranus exceeded the critical value required to produce a long-lived, insulating condensation zone, but the same was not true for Neptune, then Uranus' outer convective envelope may have cooled more quickly than that of Neptune, explaining the dichotomy. This would then constitute a prediction about the respective water abundances in Uranus and Neptune that could be tested by future missions. Alternatively, the water abundance may have been above the critical value in both planets, but the development of a robust gradient zone in Neptune may have been hampered by unfavorable conditions related, for example, to a different opacity profile in the planet created by different methane or ammonia abundances.

As discussed in the previous section, it is also possible that a competition may develop between formation of a stable gradient

zone and its erosion through entrainment into the overlying convective envelope during planetary cooling, producing a regime of episodic behavior, characterized by long periods of steady cooling separated by sudden outbursts of increased convective activity and heat release. If such a scenario were indeed operating in the ice giants, then Uranus, with its low internal heat flux, might currently be in a state of steady cooling while Neptune may be going through a state of heightened convective activity. However, given the limited supply of energy being tapped and the efficiency with which convection transfers heat, the periods of high activity would necessarily be relatively short-lived, and consequently the probability that we are living during such an epoch is presumably fairly low. Nevertheless, we cannot dismiss the possibility that the dichotomy in the measured internal heat fluxes from the two planets may be a sign of unsteadiness in the heat release rates from their interiors.

It is essential to have good cooling models of the ice giants, because these models bolster our understanding of how they formed and what their internal structures are like. Including the effects of water condensation in cooling models of the ice giants could potentially alleviate the disagreement between the model predictions for Uranus' current effective temperature and its observed value (Fortney et al., 2011; Nettelmann et al., 2013). On the other hand, it could also adversely affect the current good agreement between the models and data for Neptune. This finding would also be important, however, since it would imply that gaps may still remain in our understanding of Neptune's cooling history. Either way, inhibition of convection in the saturated water layer may well have had an important effect on the cooling rates and should be studied in conjunction with the next generation of thermal evolution models.

The results of this study may also have interesting implications regarding the dynamics of moist convection associated with methane clouds in Uranus and Neptune and water clouds in Saturn (Guillot 1995; Li and Ingersoll 2015), where vertical stratification in the mean molecular weight could produce local stability in the condensation layer. However, because these clouds form much closer to the planetary photosphere, at pressure levels which are optically much thinner than those of the water condensation zone in the ice giants, radiative heat transfer through the layer becomes so efficient that it loses its effectiveness as an insulator. Under these circumstances, the formation of a stable gradient in such a condensation zone is unlikely to have more than a minor, if any, influence on the thermal evolution of the planet. Cyclic or episodic releases of heat and outbursts of cloud activity may be possible on short time scales, however.

Acknowledgements

The authors are indebted to Michael Flasar and an anonymous reviewer for their perceptive reviews. This research was supported by grants from the NASA Outer Planets Research Program and NASA Solar System Workings Program. It was carried out at the Jet Propulsion Laboratory, California Institute of Technology, under a contract with the National Aeronautics and Space Administration. Government sponsorship acknowledged.

Appendix A

In this section, we derive Eqs. (2) and (3) of Section 2, which provide the criteria for the local convective stability of a saturated water layer to upward and downward displacements, respectively. As pointed out by Guillot (1995), a saturated layer corresponds to the condition most prone to convection. A saturated plume penetrating an unsaturated environment will encounter a more stable compositional gradient than it would if the environment were saturated. An unsaturated plume may be positively buoyant in a saturated environment, but the subsequent mixing will ultimately act to redistribute mass in the system until the heavier condensable species collects and forms a saturated layer at the bottom of the cloud layer. Consequently, the most relevant problem reverts to the stability of a saturated zone.

In the derivation of the following equations, we ignore diffusive processes. We additionally assume that any condensed particles precipitate rapidly out of the system and make a negligible contribution to the mass density of the displaced fluid element, hence $l = 0$. The opposite extreme, in which the condensate moves with the fluid parcel without significant sedimentation, is discussed at the end of this section.

The fractional change in density of a fluid parcel displaced vertically upward by an amount δz from its equilibrium position z_0 in a pseudoadiabatic process is given by

$$\left(\frac{\delta\rho}{\rho}\right)_{pa} \simeq -\frac{\delta T}{T_0} + \frac{\delta p}{p_0} - \zeta\delta q, \tag{A1}$$

where again $\zeta \equiv \xi/(1+\xi q_0)$ and the subscript "pa" stands for "pseudoadiabatic". This expression follows directly from (1f) with $f_c = 1$. In a pseudoadiabatic process, the moist static energy resulting from a small displacement is conserved following the motion, that is, $\delta h = 0$, where δh is given by

$$\delta h = C_p\delta T + g\delta z + L\delta q/(1-q_0)$$

Using this to substitute for the temperature change in (A1) and noting that the specific humidity in a saturated parcel changes with temperature and pressure according to $\delta q = \epsilon\gamma\delta T/T_0 + \beta\delta p/p_0$ allows us to write

$$\left(\frac{\delta\rho}{\rho}\right)_{pa} \simeq \frac{(1+\varepsilon\gamma\zeta)}{1+\gamma'}\frac{\Gamma_d\delta z}{T_0} + \frac{\beta/(1-q_0)}{1+\gamma'}\left[\frac{1}{\epsilon} - (1-q_0)\zeta\right]\frac{\delta p}{p_0} + \frac{\delta p}{p_0}. \tag{A2}$$

Here, $\epsilon \equiv C_pT_0/L$, $\gamma \equiv L/C_p(\partial q_s/\partial T)_p$, $\beta \equiv p_0(\partial q_s/\partial p)_T = -q_s\frac{p}{p-(1-\varepsilon_v)e_s}$, $e_s(T)$ being the saturation vapor pressure; $\Gamma_d = g/C_p$ is the dry adiabatic lapse rate, and $\gamma' = \gamma/(1-q_0)$. Note that in this expression, we assume that the change in pressure over δz equals that of the environment, since any significant difference between the parcel and environmental pressures would be rapidly removed by acoustic relaxation over the timescale of the parcel motion.

Similarly, the change in the density of the environment with temperature profile $T_0(z)$ and pressure profile $p_0(z)$, over a distance δz, can be derived from Eq. (1f) and we find

$$\left(\frac{\delta\rho}{\rho}\right)_e \simeq -\delta z\left\{\frac{1+\epsilon\gamma\zeta}{T_0}\frac{\partial T_0}{\partial z} - \frac{1-\beta\zeta}{p_0}\frac{\partial p_0}{\partial z}\right\}. \tag{A3}$$

The buoyancy force exerted on the parcel is given by

$$B = -g\left\{\left(\frac{\delta\rho}{\rho}\right)_p - \left(\frac{\delta\rho}{\rho}\right)_e\right\}. \tag{A4}$$

Substituting (A2) and (A3) into (A4) we obtain

$$B = -\frac{g\alpha}{T}\left\{\frac{\partial T_0}{\partial z} + \Gamma_s\right\}\delta z, \tag{A5}$$

where

$$\alpha = 1 + \epsilon\gamma\zeta \tag{A6}$$

and Γ_s is the moist adiabatic lapse rate. In deriving (A5), we have used the fact that

$$\Gamma_s = \Gamma_d\frac{1-q_0-l-\beta L/RT_0}{1-q_0-l+\gamma} \tag{A7}$$

The presence of non-zero l in (A7) is correct only for the slow-precipitation limit; however, the formula is also correct for the fast-precipitation limit when $l = 0$ (Gill 1982). In addition, we have used the hydrostatic equation in terms of Γ_d,

$$1/p_0(\partial p_0/\partial z) = -C_p\Gamma_d/RT_0$$

In the neighborhood of T_0, the saturation specific humidity varies as

$$q_s \cong a\,\exp\left\{-\frac{L}{R_w}\left(\frac{1}{T}-\frac{1}{T_0}\right)\right\}. \tag{A8}$$

R_w is the gas constant of pure water. Consequently,

$$\epsilon\gamma = (q_sL/R_wT_0)\frac{1+\xi q_s - l(1-f_c)}{1-(q_s+l)(1-f_c)}$$

where we have formulated this expression to be correct for both the fast- ($f_c = 1$) and slow- ($f_c = 0$) precipitation limits. Substituting this into (A6) with $f_c = 1$ we obtain

$$\alpha = 1 + \xi\,(q_sL/R_wT_0) \tag{A9}$$

This is the form of α given in Section 2. The parameter α is negative when q_s is greater than $-R_wT_0/\xi L$. Eq. (A5) shows that when α is negative, the saturated layer is stable to an upward parcel displacement (B and δz have opposite signs) when the lapse rate is *superadiabatic* with respect to the moist adiabat, counter to our experience with moist convection in Earth's atmosphere. The difference is attributable to the high ratio of the molecular weight of water to that of the hydrogen-helium mixture in the ice giants.

The stability criterion for a parcel displaced downward is different because there is no condensation of vapor, and in the limit where the condensate precipitates out rapidly, no evaporation either. The specific humidity of the parcel is therefore conserved during the downward displacement. In this case, (A2) takes the simple form

$$\left(\frac{\delta\rho}{\rho}\right)_{pa} = \frac{\Gamma_d\delta z}{T_0} + \frac{\delta p}{p_0} \tag{A10}$$

and the difference between this and (A3) leads to the expression

$$B = -\frac{g}{T}\left\{\alpha\frac{\partial T_0}{\partial z} + \left(1-\frac{C_p}{R}\beta\zeta\right)\Gamma_d\right\}\delta z, \tag{A11}$$

for the buoyancy force induced by a downward displacement in a saturated layer. For stability, B and δz must have opposite signs and thus the term in brackets must be positive, that is

$$\alpha\frac{\partial T_0}{\partial z} + \left(1-\frac{C_p}{R}\beta\zeta\right)\Gamma_d > 0 \tag{A12}$$

This is the basis for the stability diagram shown in Fig. 2. It is straightforward to show that Eq. (A12) corresponds to the Ledoux criterion (Ledoux 1947) for the convective stability of a layer possessing a mean molecular weight gradient, where in this case the gradient is provided by the saturation profile of water in a hydrogen-dominated atmosphere.

Finally, we derive the stability criterion for the case where condensate precipitation is slow and particles follow the fluid motion during the displacement. This regime is favored for high pressures and small particle sizes. Again, we assume that the environment is free of particles, a reasonable assumption if the layer is found to be stable, since convective motions are presumably required to maintain a cloudy layer over a long time. Because there are initially no particles in the test parcel, it is clear that the stability criteria for upward and downward displacements must be treated separately. (When the test parcel is displaced upward from the equilibrium position, it will form and retain particles; when displaced downward, it will not, nor are there any particles available to evaporate.) The specific humidity of the parcel initially equals the saturated value q_0 at the equilibrium level. As it rises, it remains saturated and a mass mixing ratio $l = q_0 - q_s$ of the condensed phase is produced, where q_s is the local saturation humidity at the level of the parcel. This follows from mass conservation and the stipulation that no mass is exchanged with the environment. Following the steps that led to (A12) but now assuming that total water is conserved in the parcel, we find the layer will be stable to an *upward displacement* if

$$\alpha\frac{\partial T_0}{\partial z} + \left\{\alpha\frac{\Gamma_s}{\Gamma_d} + \frac{1}{1+\gamma'}\left[\frac{q_0L}{R_wT_0} + \frac{\beta C_p}{R(1+\xi q_0)}\right]\right\}\Gamma_d > 0 \tag{A13}$$

Since this is a fairly complicated expression, we present a numerical example to better illuminate its implications. We evaluate the term in brackets in (A13) for a case in which $q_0 = 0.25$ for a temperature $T_0 = 450$ K. For these conditions, $\alpha \approx -1.26$, $q_0L/R_wT_0 \approx 2.6$, $\gamma' \approx 1.86$, and $\beta \approx -0.25$. We also find $C_p/R \approx 2.5$. Hence the second term in the brackets is approximately equal to 0.63. In addition, for these conditions, $\Gamma_s/\Gamma_d \approx 0.55$. We thus see that the two terms in the bracket nearly cancel. Hence, for this case stability against an upward displacement requires $\partial T_0/\partial z$ to be negative but the lapse rate corresponding to neutral stability could be much less than the dry adiabatic value. It is straightforward to see that the stability criterion for a *downward displacement* for the assumptions adopted is given by (A12).

Appendix B

To derive the overstability condition for oscillatory diffusive convection in the water condensation zone, we begin with Eqs. (1a)–(1g) of Section 2. We derive this condition under the assumptions that the vertical shear of the mean zonal wind is zero (and therefore, without loss of generality, we can regard the background state as motionless); that the background mean state is hydrostatic; and that the viscosity ν and radiative diffusivity κ_r can be regarded as constant with height over the depth of the layer. We also assume that fluid parcels remain close to saturation, such that to a good approximation the perturbation specific humidity $q' = \epsilon\gamma T'/T_0 + \beta p'/p_0$, with T', p' the perturbation temperature and pressure and T_0, p_0 the local background temperature and pressure. This requires that condensed droplets evaporate in the downdrafts before they can precipitate out of the system.

The general steps in the derivation mirror those presented in Chapter 6 of Gill (1982) in the discussion of the adjustment to equilibrium in a stratified compressible fluid, but with the inclusion of the effects of condensation. We start by substituting the above expression for q' into (1f), eliminating dT'/dt between (1e) and (1f), and substituting the resulting expression for $d\rho'/dt$ into (1d). This results in an equation relating u', w', T', and P'. We then eliminate u' from this equation using (1a). Taking the time derivative of (1c) and eliminating $d\rho'/dt$ yields an independent equation relating w', T', and P'.

We look for normal-mode solutions of these equations. We express (w', T') in the form $(w', T') = \rho_0^{-1/2}(\boldsymbol{W},\ \boldsymbol{T})e^{i(kx+mz-\omega t)}$ and p' in the form $p' = \rho_0^{1/2}\boldsymbol{P}e^{i(kx+mz-\omega t)}$, where $\boldsymbol{W}$, $\boldsymbol{T}$, and $\boldsymbol{P}$ represent complex Fourier amplitudes, and the solutions correspond to the real parts of these expressions. Substituting these forms into the two independent equations yields two new equations coupling $\boldsymbol{W}$, $\boldsymbol{T}$, and $\boldsymbol{P}$. Next, $\boldsymbol{T}$ can be expressed in terms of $\boldsymbol{W}$ and $\boldsymbol{P}$ by taking the Fourier transform of (1e) after eliminating q' using (1g) and the saturation condition. Eliminating $\boldsymbol{T}$, we arrive at a coupled system of two equations in the two unknowns $\boldsymbol{W}$ and $\boldsymbol{P}$:

$$\begin{bmatrix} M_{11} & M_{12} \\ M_{21} & M_{22} \end{bmatrix}\begin{bmatrix} \boldsymbol{P} \\ \boldsymbol{W} \end{bmatrix} = 0 \tag{B1}$$

where

$$M_{11} = -k^2 - i\omega L_{\omega,\upsilon}\frac{A}{g} + i\omega\frac{L_{\omega,\upsilon}}{L_{\omega,\kappa}}D_P^1 \tag{B2a}$$

$$M_{12} = -L_{\omega,\upsilon}\left(im + \frac{1}{2H_\rho} + A\right) + \frac{L_{\omega,\upsilon}}{L_{\omega,\kappa}} D_W^1 \tag{B2b}$$

$$M_{21} = i\omega\left(im - \frac{1}{2H_\rho} - A\right) + \frac{i\omega}{L_{\omega,\kappa}} D_P^2 \tag{B2c}$$

$$M_{22} = i\omega L_{\omega,\upsilon} - g\left(\frac{1}{H_\rho} + A\right) + \frac{1}{L_{\omega,\kappa}} D_W^2 \tag{B2d}$$

are the matrix coefficients of the linear system. Other definitions include:

$$L_{\omega,\upsilon} = -i\omega + \nu K^2$$

$$L_{\omega,\kappa} = -i\omega + \frac{\kappa_r}{1+\gamma'} K^2$$

and

$$K^2 \equiv k^2 + m^2 + \frac{1}{4H_\rho^2}$$

H_ρ being the density scale height. The static stability of the layer is expressed through the parameter A:

$$A = \frac{\alpha_c \Gamma_s}{T_0} - \frac{1}{H}\left(1 - \beta \frac{1 - f_c + \xi}{1 + \xi q - l(1 - f_c)}\right) = \frac{N_\alpha^2}{g} - \frac{1}{H_\rho} \tag{B3}$$

where the expression on the right serves to define an associated buoyancy frequency N_α, which reduces to the usual Brunt frequency when $\alpha = 1$. The parameter α_c is given by

$$\alpha_c = 1 + \frac{(1 - f_c + \xi)\epsilon\gamma}{1 + \xi q - l(1 - f_c)}$$

This reduces to $\alpha_c = \alpha$ when $f_c = 1$. It is also worth noting that when $f_c = 1$,

$$\frac{1}{H_\rho} = \frac{\alpha}{T_0}\frac{dT_0}{dz} + \frac{1}{H_0}\{1 - \beta\zeta\}$$

when the background saturated water profile is included, while

$$A = \frac{\alpha}{T_0}\Gamma_s - \frac{1}{H_0}\{1 - \beta\zeta\}$$

where H_0 is the pressure scale height. Hence, by (B3), we see that

$$\frac{N_\alpha^2}{g} = \frac{\alpha}{T_0}\left(\frac{dT_0}{dz} + \Gamma_s\right)$$

which shows that the stability criterion given in (2) is equivalent to $N_\alpha^2 > 0$.

The effects of viscosity and radiative diffusion enter through the parameters D_P^1, D_P^2, D_W^1, and D_W^2 given by

$$D_P^1 = \frac{D_P^2}{g} = \frac{\alpha_c \kappa_r K^2}{1+\gamma'}\frac{\Gamma_s}{gT_0} \tag{B4a}$$

$$D_W^1 = \frac{D_W^2}{g} = \frac{\alpha_c \kappa_r K^2}{1+\gamma'}\frac{N_0^2}{g} \tag{B4b}$$

where $N_0^2 = \frac{g}{T_0}\left(\frac{\partial T_0}{\partial z} + \Gamma_s\right)$ and $\gamma' \equiv \gamma/(1 - q_0)$. Note that N_0^2 is negative in the superadiabatic gradient zone.

Nontrivial solutions to the homogeneous linear system (B1) exist only when the determinant of the matrix vanishes. This yields the dispersion relation for small-amplitude disturbances:

$$-i\omega L_{\omega,\upsilon}\left\{K^2 + i\omega L_{\omega,\upsilon}\frac{A}{g} + \frac{1}{L_{\omega,\kappa}}\left[\left(D_W^1 - D_P^2\right)\left(im - \frac{1}{2H_\rho}\right) - i\omega L_{\omega,\upsilon} D_P^1\right]\right\} + k^2\left(N_\alpha^2 - \frac{D_W^2}{L_{\omega,\kappa}}\right) = 0 \tag{B5}$$

The above expression can be simplified somewhat by noting that it includes terms associated with acoustic modes (modified by buoyancy) in addition to buoyancy modes. Since the diffusive convection occurs at very low Mach number, the acoustic modes contain little energy and are of little interest. We filter out these modes by dropping the second term in the brackets (proportional to A/g) and the term proportional to D_P^1.

Next, it is useful to non-dimensionalize (B5) by introducing the following definitions:

$$\omega' = \omega/N_\alpha \cos\chi$$

$$\eta = \frac{DK^2}{N_\alpha \cos\chi}$$

$$\delta = -\left(imH_\rho - \frac{1}{2}\right)\left(\frac{H_\rho}{H} - 1\right)\frac{D}{(1+\gamma')H_\rho^2 N_\alpha \cos\chi}$$

where $\cos\chi = k/K$ and D is the effective diffusivity defined in Section 3. The parameter δ expresses the influence on the overall buoyancy of diffusion of heat and moisture down the basic-state gradients. We also introduce the definition $r_N = N_\alpha^2/N_0^2$. (Note that r_N is negative in the superadiabatic gradient zone since $N_\alpha^2 > 0$ and $N_0^2 < 0$ in the layer.) With these definitions, the dispersion relation can be written in the final form

$$\sigma^3 + \left[\left(1 + \mathrm{P}'\right)\eta + \alpha_c\delta\right]\sigma^2 + \left(1 + \mathrm{P}'\eta^2 + \mathrm{P}'\eta\alpha_c\delta\right)\sigma + \left(1 - \frac{\alpha_c}{r_N}\right)\eta = 0 \tag{B6}$$

where $\sigma = -i\omega'$, $\mathrm{P}' = \frac{1+\gamma'}{1+\gamma'\tau}\mathrm{Pr}$, and $\tau = D_q/\kappa_r$ is the diffusivity ratio. In the limit of no diffusion, (B6) reduces to $\sigma^3 + \sigma = 0$, which has the trivial root zero and two roots corresponding to $\omega^2 = N_\alpha^2 \cos^2\chi$. ω must be real for stable solutions. Hence, in the zero-diffusion limit, we recover the usual requirement for stability that $N_\alpha^2 > 0$, and the discussion following (B3) shows that we also recover (2) in the rapid precipitation limit.

The dispersion relation (B6) includes the effects of finite pressure and temperature scale height, as well as the effect of pressure on the saturation humidity (through B3), and it is valid in both the fast and slow precipitation limits. It is derived under the assumption that saturation equilibrium is quasi-statically maintained at all times. It therefore should reduce to the dispersion relation found by Leconte et al. (2017) for the same limit, that is, the "efficient condensation limit" (see their Eq. (47)), after all the approximations they make in their derivation are incorporated into (B6). We have verified that this is in fact the case. Recovering Leconte et al.'s assumption of rapid removal of condensate means we must set $f_c = 1$ and $l = 0$ in our equations, and their neglect of the effect of pressure on saturation equilibrium means we should take $\beta = 0$. In addition, to recreate their use of the Boussinesq approximation and their focus on the "elevator mode" ($\chi = 0$), we must take the limit of infinite pressure and temperature scale heights and set the vertical wavenumber m to zero. Hence, $\delta \to 0$ and it drops out of (B6). It can also be seen from (B3) and the expressions that follow that $N_\alpha^2 = \alpha N_0^2$ and $\alpha_c = \alpha$ when $f_c = 1$. Consequently, the last term in (B6) vanishes and (B6) collapses to a quadratic equation, as it must to agree with Eq. (47) of Leconte et al. (2017) After imposing all these limits in (B6), it becomes straightforward to verify that the two dispersion relations are the same, although some effort must be expended to overcome the differences in notation, parameter definitions, and non-dimensionalization.

We have also confirmed that our methods recover the stability criterion for dry diffusive convection in the Boussinesq approximation. Briefly, we use the same methods as for the normal analysis presented above, with all terms related to condensation set to zero, and with a fractional mean molecular weight gradient controlled by $-\zeta\, dq_0/dz$, where q_0 is now arbitrary, as opposed to be-

ing controlled by saturation equilibrium. However, we must dispense with the formulae given in (B2), since the assumption of saturation equilibrium relating humidity to temperature perturbations was made at the outset to derive them. Instead, we must add q' as a dependent variable. This introduces an additional Fourier amplitude **q** to the prior set, which is eventually expressed in terms of $\boldsymbol{W}$ using (1g) with $E = C = 0$. We find the resulting dispersion relation matches Eq. (8.1.8) of Turner (1973) if we identify his RaPr with our $-N_0^2(d^4/\kappa_r^2)$ and RsPr with our $g\zeta(dq_0/dz)(d^4/\kappa_r^2)$, where Ra and Rs are the thermal and compositional Rayleigh numbers employed in Turner's analysis. The reasons for making these identifications should be clear after considering that N_0^2 is a measure of the thermal static stability gradient (see the expression following B4) whereas $\zeta(dq_0/dz)$ is a measure of the compositional stability gradient.

The growth rate of a linear perturbation is given by the real part of σ. The maximum growth rate for given wavelength parameter η is found as the maximum among the real parts of the three roots of (B6). Fig. 3 presents the maximum growth rate for diffusive-convective instability as a function of η for $\mathrm{Pr} = 0.05$ and $\mathrm{Pr} = 0.4$. For the case shown, the lapse rate in the gradient zone was assumed to be $2\Gamma_d$, where Γ_d is the dry adiabatic lapse rate. Additional calculations showed that the maximum growth rates are insensitive to the lapse rate of the gradient zone. For example, the results for lapse rates of $2\Gamma_d$ and $40\Gamma_d$ differ only in detail, while the basic conclusions expressed in the text are unchanged.

References

Asplund, M., Grevesse, N., Sauval, A.J., Scott, P., 2009. The chemical composition of the Sun. Annu. Rev. Astron. Astrophys. 47, 481–522.

Atreya, S.K., Mahaffy, P.R., Niemann, H.B., Wong, M.H., Owen, T.C., 2003. Composition and origin of the atmosphere of Jupiter: an update, and implications for the extrasolar giant planets. Planet. Space Sci. 51, 105–112.

Baines, K.H., Hammel, H.B., Rages, K.A., Romani, P.N., Samuelson, R.E., 1995. Clouds and haze in the atmosphere of Neptune. In: Cruikshank, D.P. (Ed.), Neptune and Triton. U. Arizona Press, Tucson, pp. 489–546.

Bergman, T.L., Incropera, F.P., Viskanta, R., 1986. Correlation of mixed layer growth in a double-diffusive, salt-stratified system heated from below. Trans. ASME 108, 206–211.

Briggs, F.H., Sackett, P.D., 1989. Radio observations of Saturn as a probe of its atmosphere and cloud structure. Icarus 80, 77–103.

Carpenter, J.R., Sommer, T., Wüest, A., 2012. Simulations of a double-diffusive interface in the diffusive convection regime. J. Fluid Mech. 711, 411–436.

Conrath, B.J., Gierasch, P.J., 1984. Global variation of the para hydrogen fraction in Jupiter's atmosphere and implications for dynamics on the outer planets. Icarus 57, 184–204.

Forsythe, W.E., et al., 1954. Smithsonian Physical Tables (9th Revised Edition). Knovel Press.

Fortney, J.J., Nettelmann, N., 2010. The interior structure, composition, and evolution of giant planets. Space Sci. Rev. 152, 423–447.

Fortney, J.J., Ikoma, M., Nettelmann, N., Guillot, T., Marley, M.S., 2011. Self-consistent model atmospheres and the cooling of the solar system's giant planets. Ap. J. 729, 32–45.

Gill, A.E., 1982. Atmosphere-Ocean Dynamics. Academic Press, San Diego, CA.

Guillot, T., Gautier, D., Chabrier, G., Mosser, B., 1994. Are the giant planets fully convective? Icarus 112, 337–353.

Guillot, T., 1995. Condensation of methane, ammonia, and water and the inhibition of convection in the giant planets. Science 269, 1697–1699.

Hubbard, W.B., MacFarlane, J.J., 1980. Structure and evolution of Uranus and Neptune. J. Geophys. Res. 85. doi:10.1029/0JGREA0000850000B1000225000001.

Hubbard, W.B., Podolak, M., Stevenson, D.J., 1995. The interior of Neptune. In: Cruikshank, D.P. (Ed.), Neptune and Triton. U. Arizona Press, Tucson, pp. 109–140.

Hull, J.R., Nielsen, C.E., Golding, P., 1989. Salt-Gradient Solar Ponds. CRC Press, Florida.

Huppert, H.E., Turner, J.S., 1981. Double-diffusive convection. J. Fluid Mech. 106, 299–329.

Leconte, J., Selsis, F., Hersant, F., Guillot, T., 2017. Condensation-inhibited convection in hydrogen-rich atmospheres: stability against double-diffusive processes and thermal profiles for Jupiter, Saturn, Uranus, and Neptune. Astron. Astrophys 598 A98. doi:10.1051/0004-6361/201629140.

Ledoux, W.P., 1947. Stellar models with convection and with discontinuity of the mean molecular weight. Ap. J. 105, 305.

Li, C., Ingersoll, A.P., 2015. Moist convection in hydrogen atmospheres and the frequency of Saturn's giant storms. Nat. Geosci. 8, 398–403.

Lindal, G.F., Lyons, J.R., Sweetnam, D.N., Eshleman, V.R., Hinson, D.P., Tyler, G.L., 1987. The atmosphere of Uranus: Results of radio occultation measurements with Voyager 2. J. Geophys. Res. 92, 14987–15001.

Linden, P.F., Shirtcliffe, T.G.L., 1978. The diffusive interface in double-diffusive convection. J. Fluid Mech. 87, 417–432.

Marrero, T.R., Mason, E.A., 1972. Gaseous diffusion coefficients. J. Phys. Chem. Ref. Data 1, 3.

Mirouh, G.M., Garaud, P., Stellmach, S., Traxler, A.L., Wood, T.S., 2012. A new model for mixing by double-diffusive convection (semi-convection): I. The conditions for layer formation. Ap. J. 750, 61–78.

Nettelmann, N., Helled, R., Fortney, J.J., Redmer, R., 2013. New indication for a dichotomy in the interior structure of Uranus and Neptune from the application of modified shape and rotation data. Planet. Space Sci. 77, 143–151.

Nielsen, C., 1979. Control of gradient zone boundaries. In: Proceedings of the Silver Jubilee Congress. Pergamon Press, Atlanta, GA.

Pearl, J.C., Conrath, B.J., 1991. The albedo, effective temperature, and energy balance of Neptune. J. Geophys. Res. 96, 18921.

Podolak, M., Hubbard, W.B., Stevenson, D.J., 1991. Models of Uranus' interior and magnetic field. In: Bergstralh, J.T., Miner, E.D., Matthews, M.S. (Eds.), Uranus. U. Arizonal Press, Tucson.

Radko, T., 2003. A mechanism for layer formation in a double-diffusive fluid. J. Fluid Mech. 497, 365–380.

Rosenblum, E., Garaud, P., Traxler, A., Stellmach, S., 2011. Turbulent mixing and layer formation in double-diffusive convection: three-dimensional numerical simulations and theory. Ap. J. 731, 66.

Spiegel, E.A., Veronis, G., 1960. On the Boussinesq approximation for a compressible fluid. Ap. J. 131, 442–447.

Sreenivas, K.R., Arakeri, J.H., Srinivasan, J., 1995. Modeling the dynamics of the mixed layer in solar ponds. Solar Energy 54, 193–202.

Sromovsky, L.A., Fry, P.M, Kim, J.H., 2011. Methane on Uranus: the case for a compact CH_4 cloud layer at low latitudes and a severe CH_4 depletion at high-latitudes based on re-analysis of Voyager occultation measurements and STIS spectroscopy. Icarus 215, 292–312.

Suárez, F., Tyler, S.W., Childress, A.E., 2010. A fully-coupled, transient double-diffusive convective model for salt-gradient solar ponds. Int. J. Heat Mass Transfer 53, 1718–1730.

Tritton, D.J., 1977. Physical Fluid Dynamics. Van Nostrand Reinhold, United Kingdom.

Turner, J.S., 1973. Buoyancy Effects in Fluids. Cambridge University Press, Cambridge.

Wood, T.S., Garaud, P., Stellmach, S., 2013. A new model for mixing by double-diffusive convection (semi-convection): II. Transport Heat Compos. Layers. Ap. J. 768, 157–170.

Zhang, G.J., McFarlane, N.A., 1995. Sensitivity of climate simulations to the parameterization of cumulus convection in the Canadian Climate Center general circulation model. Atmos. Ocean 33, 407–446.